UNIVERSITÀ DEGLI STUDI DI PAVIA

DOTTORATO IN SCIENZE CHIMICHE E FARMACEUTICHE

XXX CICLO

Coordinatore: Chiar.mo Prof. Mauro Freccero

APPLICATION OF NEUTRON ACTIVATION ANALYSIS FOR THE CHARACTERIZATION OF THE SILICON MATERIAL USED TO DETERMINE THE AVOGADRO CONSTANT

Tutori

Chiar.mo Prof. Massimo Oddone

Chiar.mo Dott. Giancarlo D'Agostino

Tesi di Dottorato di

MARCO DI LUZIO

a.a. 2016- 2017

1. Introduction

1.1 Metre convention

The process to assign an interval of values to a measurand, the quantity of interest, is called measurement[1] and is fundamental in almost every field of science as well as everyday life. An important information retrieved from the measurement process is a numerical value assessing the ratio of the measurand to a reference dimension that have to be stated.

In the last centuries scientists and traders tried to make arrangements for the application of a set of shared references and consequently, different systems of units of measurement spread out.

At the end of 19^{th} century, effort to set homogeneous and consistent units of measurement, in order to be recognized and used in every part of the world, led to formal agreement between governments of 17 defined "Member States" and signature of the metre convention in 1875. Main content of the convention concerned the institution of a *Bureau International de poids et mesures* (BIPM), an organization with the task to store the (official) international prototype artifacts of metre and kilogram and compare them with their national copies to allow and maintain over time a correct dissemination of standard units of measurement.[2]

The system of measurement containing as length and mass units the metre [m] and kilogram [kg] prototypes defined in the 1875 convention, and often referred to as metric system, was chosen as the International System of units of measurement (SI) adopted as world-wide reference.

In the following years, BIPM committees met at regular intervals proposing and discussing possible changes; as a result of their work, other units of measurement were included in the SI to reach the current number of 7 base units. Units of time, second [s], electric current, ampere [A], thermodynamic temperature, kelvin [K], luminous intensity, candela [cd], and amount of substance, mole [mol], were added to length [m] and mass [kg] units already discussed.

The most recent introduction of mole, occurred only in 1971, was very controversial and followed a long discussion between chemists and physicists. Agreement was reached among International Unions of Physics and Chemistry (IUPAP and IUPAC, respectively) and International Organization for Standardization (ISO) leading to the current convention based on the relative atomic mass of ^{12}C.

SI defines also a large amount of derived units that can be entirely expressed in terms of the seven base units (area, [m^2], volume [m^3], speed [m s^{-1}], force [kg m s^{-2}, called newton], pressure [kg m^{-1} s^{-2}, called pascal], potential difference [kg m^2 s^{-3} A^{-1}, called volt], just to cite the most used). To express different orders of magnitude of SI units, prefixes are introduced in the range from 10^{24} (prefix yotta, Y) to 10^{-24} (prefix yocto, y). Non SI units that are common in particular fields (angstrom for length or bar for pressure) are tolerated, however their use is warmly not recommended by BIPM.

1.2 Redefinition of SI

Each unit of measurement included in the SI is described with a definition, a sentence that unequivocally identifies it. While the most part of units are currently defined on well-known fundamental physical constants, there is one unit still referred to a material artifact. An example of the first group corresponds to the current definition of the second:

> *"The second is the duration of 9192631770 periods of the radiation corresponding to the transition between the two hyperfine levels of the ground state of the caesium 133 atom."*[3]

On the other hand, the kilogram is defined as follows:

> *"The kilogram is the unit of mass; it is equal to the mass of the international prototype of the kilogram."*[3]

The international prototype of kilogram is the Ir-Pt alloy cylinder maintained at the BIPM. It was manufactured, in consequence of the metre convention, as an exact copy of the "kilogram of the Achives", a Pt artifact which mass was a thousand times that of 1 cm^3 of water at temperature of 4 °C, produced during the French revolution, kept in the Archives of the Republic and considered as the mass standard for that time in France.

The kilogram definition implies that all mass measurements performed in the world are strictly related and referred to a metal boule kept in a vault stored in the basement of a building placed in a suburb of Paris. Despite the mass of the international prototype is exactly 1 kg by definition, because of its material nature, we cannot rely on its absolute stability; in fact the third periodic verification performed at the end of the last century pointed out discrepancies among the prototype, its official copies and its national copies.[4,5]

The instability of the kilogram affects traceability of all mass measurements to the mass standard but also reflects on the derived units that rely on it; in conclusion, variability of the unit of mass, even in the order of few µg over more than a century, is not tolerable.

The International Commettee for Weigths and Measures (CIPM), proposed to redefine all the base units of measurement on exact fixed values of physical constants of nature. Seven constants were chosen in such a way that any unit in the new SI can be written either through a defining constant itself or through products or ratios of defining constants. In particular, second, meter and candela will rely on the hyperfine transition frequency of ^{133}Cs ($\Delta\nu^{133}Cs$), speed of light in vacuum (c) and luminous efficacy (K_{cd}) of a defined monochromatic radiation, respectively (no substantial change in comparison to present SI), while kilogram, ampere, kelvin and mole will be redefined on precise values of Planck constant (h), elementary charge (e), Boltzmann constant (k) and Avogadro constant (N_A), respectively.(Figure 1)

Figure 1: Illustration of 7 base units of SI with (in clearer version of the same color) the corresponding constant on which each definition will be based.[6]

The approval for the move of SI is foreseen during the next 26th meeting of *Conference General de Poids et Mesures* (CGPM) planned in November 2018.

The advantage of the SI shift consists in the stability of the newly defined units, as physical constants of nature (as well as invariant conventional values[7,8]) are not supposed to change; moreover, a fixed value of them is used, that means they are exactly defined with no uncertainty. In addition, every laboratory in the world will have, according to its measurement capability, the possibility to manufacture his own copy of SI unit (practical realization of a SI unit definition is called *mise en pratique*).

1.3 Kilogram and mole

The definition of kg will change accordingly:

> *"The kilogram, symbol kg, is the SI unit for mass; its magnitude is set by fixing the numerical value of the Planck constant to be exactly 6.626069**X** × 10^{-34} when it is expressed in the SI unit for action J s = kg m^2 s^{-1}."*[9]

In the revised SI, kg will be defined with a fixed value of *h* (bold X indicates that further digits are still to be set before redefinition) together with knowledge of *c*, defining m, and $\Delta\nu^{133}$Cs, defining s, also fixed within the 2018 revision.

However, h is strictly linked to N_A through the relation leading to the well-known molar Planck constant ($N_A h$), knowledge of $N_A h$ allows then easily to switch from h to N_A and vice versa without losing uncertainty on the determination. For that reason, two synergic approaches to determine h are possible: directly by Kibble balance[10] experiment or indirectly by the X-ray crystal density (XRCD) method on a suitable sample and following conversion exploiting $N_A h$.

The CIPM chose to complementarily examine both Kibble balance and XRCD pathways to accomplish determination of h, and consequently move kg definition, only when the two approaches will result in values compatible to each other within 2×10^{-8} relative uncertainty.

The base unit of amount of substance will be redefined as indicated below:

> *"The mole, symbol mol, is the SI unit of amount of substance of a specified elementary entity, which may be an atom, molecule, ion, electron, any other particle or a specified group of such particles; its magnitude is set by fixing the numerical value of the Avogadro constant N_A to be $6.0221412\mathbf{X} \times 10^{23}$ when expressed in the SI unit mol^{-1}."*[9]

With the proposed definition, amount of substance will be exactly a fixed number of entities. For that reason, the determination of N_A plays an important role within the future SI revision, as it will be the constant underneath the amount of substance unit and a key to redefine also the kilogram.

The N_A value is obtained with the XRCD method using a mono-crystalline silicon sphere highly enriched in isotope ^{28}Si[11,12]; with this technique it is possible to calculate N_A from the knowledge of the mass, m, and volume, V, of the sphere and the molar mass, M, and lattice parameter, a, of the mono-crystalline silicon according to:

$$N_A = \frac{n M V}{m a^3}, \tag{1}$$

where n is the number of atoms in the crystalline unit cell.

The mono-crystalline silicon used to manufacture the sphere has an enrichment in isotope ^{28}Si not lower than 0.9999 mol mol^{-1}. The values of the parameters in the model (eq. 1) have to be known with an uncertainty satisfying the target 2×10^{-8} standard relative uncertainty for N_A. In details, n is a constant with value of 8 atoms per cell for Si single crystal structure, a is evaluated through geometrical relationship from results of {220} lattice planes distance obtained with x-ray and optical interferometry[13], m is obtained with high precision mass comparators and corrected for the mass deficit due to bulk impurities and voids[14] (the link with the mass, in particular with the international prototype of kilogram is maintained), V is measured through sphere diameter using an optical interferometer with spherical reference faces, and M is determined considering the two depleted minor natural isotopes (^{29}Si and ^{30}Si) as trace impurities and relying on Si isotopes well-known atomic masses; a way to achieve this is by means of Induced Coupled Plasma Isotope Dilution Mass Spectrometry (ICP-IDMS)[15]. Several influence factors affect the resulting N_A value

(e.g. point defects such as, impurity elements and vacancies, lattice spacing homogeneity, surface layers contamination and surface inhomogeneity) and must be corrected for.

In this framework, a research activity based on neutron activation analysis (NAA) was carried out to solve a discrepancy among molar mass results and to determine the mass deficit of the sphere due to point defects.

The measurement models, the performed experiments and the obtained results are reported in details in chapters 2, 3, and 4 of this doctorate thesis. The structure of these chapters follows the three aims, i.e. measurements of the ^{30}Si mole fraction, bulk impurities and vacancies concentration, respectively.

2. Aim

In this chapter, fundamentals of NAA are briefly recalled before a detailed statement of the measurement models adopted to reach the three aims.

2.1 Neutron Activation Analysis

NAA is an analytical technique based on activation of stable nuclides through exposure to a neutron flux, in order to obtain radionuclides, and detection of emitted particles which can be identified relatively to their characteristic decay mode and quantified.

Activation phase occurs within defined irradiation facilities of a neutron reactor. There are different strategies to get a neutron flux and various reactor layouts; in the currently most common setup, adopted fuel (U is largely used) sustains a fission chain reaction with production of neutrons that are slowed down in the thermal range (in kinetic equilibrium with surrounding environment) by a moderator. Neutrons have a probability to interact with target isotopes. This probability is linked to a particular parameter, called cross section, σ, commonly given in barns, b, where, 1 b corresponds to 10^{-28} m^2. A typical σ exists for each kind of interaction between nuclides and neutrons: in case of neutrons in the thermal range, thermal neutron capture cross section, σ_{th}, is linked to the probability for a defined nuclide to accept a neutron with a consequent emission of prompt gammas, corresponding to the probability of (n,γ) reaction. The σ_{th} value has a typical trend that shows an inverse proportionality in relation to the square root of neutron energy. Additional interactions are also possible, each one with its typical σ but they generally represent side-reactions in the framework of a NAA analysis. The combination of cross sections and probability distribution of neutron flux in the nuclear reactor, both energy dependent, accounts for the transformation of target in the expected product per unit of time.

If during activation phase an instable isotope is formed, it will decay with a precise scheme. Decay is the pathway a radioactive isotope has to regain stability: a radionuclide try to lose energetic surplus, obtained from the capture of a neutron, in different ways; a typical strategy consists in the emission of various particles, ^{4}He nuclide, α, electrons or positrons, β^- or β^+ (involving transformation of a neutron into a proton in the first case and vice versa in the latter), and photons, γ.[16]

Probability that a given nuclide would decay depends on the observation time. However, time interval necessary to get the half of the starting amount of that nuclide is fixed and referred to as half-life ($t_{1/2}$); a valuable nuclear parameter, decay constant, λ, can be deduced from it having reciprocal unit of measurement of $t_{1/2}$ as $\lambda = \frac{\ln 2}{t_{1/2}}$. Moreover, radionuclide's emissions are finely regulated by quantum mechanics and are released in defined proportions making quantification of radioisotopes at a defined time possible from the amount of their emitted entities.

Detection phase can rely on identification of all emitted particles but is generally performed with γ-spectrometers, via detection of γ-rays following the radioactive decay of the activated isotope; in fact, γ-rays can be immediately issued during the neutron capture of the (n,γ) activation reaction, here the γ in parenthesis precisely refers to this defined "prompt" gamma, otherwise they can be emitted directly or, more likely, indirectly (consecutively to another decay type, α or β) during the radioactive decay. The delayed situation is the one exploited in NAA analysis. γ-rays have high energy, in the range from tens of keV to few MeV, and are highly penetrating in matter but can interact with detectors (HyperPure Ge crystals, HPGe, are widely used) in many ways: photoelectric effect, Compton scattering and pair production. In case the energy carried by γ-ray is deposed within the detector, the signal is transferred and collected in spectrum; when the whole energy of the incoming γ-ray is absorbed, the so-called full-energy peak appears in the spectrum. Area of full energy peak, unless interferences of gammas in coincidence, is equal to the amount of γ-rays emitted by radionuclide and integrally detected by the spectrometry chain; this is proportional to number of radionuclides through full-energy peak efficiency, ε, that represents one of the delicate parameters in the NAA analysis.

NAA is defined as radiochemical or instrumental (INAA), whether it contemplates chemical separation of activated radioisotopes or no sample dissolution at all, respectively. It is suitable for traces and ultra-traces quantification due to the very low achievable detection limits albeit they strongly depend on investigated matrix. It has all the potential to be considered as a primary method (at least when it's performed in the classic direct comparator approach). In fact, it is entirely based on solid and well-understood principles, its measurement model allows the design of a complete uncertainty budget and it is successfully used in international key comparisons.[17]

Measurement model of INAA ultimately connects the amount of target isotope to the net area of full energy peak seen in the γ-spectrum.

In the activation phase, the number of activated nuclides per second per target nucleus, i.e. the production rate per target nucleus, R, is defined as the integral of product between neutron flux and

cross section of the (n,γ) reaction over the whole neutron energy range or velocity (conversion is straightforward with kinetic energy formulae: $E = \frac{1}{2}mv^2$, with m the mass of neutron):

$$R = \int_0^\infty n(v)\,\sigma(v)\,dv, \tag{2}$$

where v is the neutron velocity, $n(v)$ is the neutron density and $\sigma(v)$ is the (n,γ) reaction cross section. As it is unpractical to deal with integrals, some approximation were introduced leading to results with appreciable reliability; in particular, Høgdahl convention and Westcott formalism were proposed. The first one introduces a split in a typical neutron flux distribution per unit of energy (Figure 2) at level of the Cd cutoff energy, E_{Cd}. ^{113}Cd isotope has a strong resonance at about 0.55 eV absorbing the almost totality of neutrons below that point. The two resulting regions are called sub-cadmium and epi-cadmium (or thermal and epithermal) and show different behavior of the distribution related to neutron energy.

Figure 2: Portions of the neutron flux in a fission reactor showed in a log-log representation.

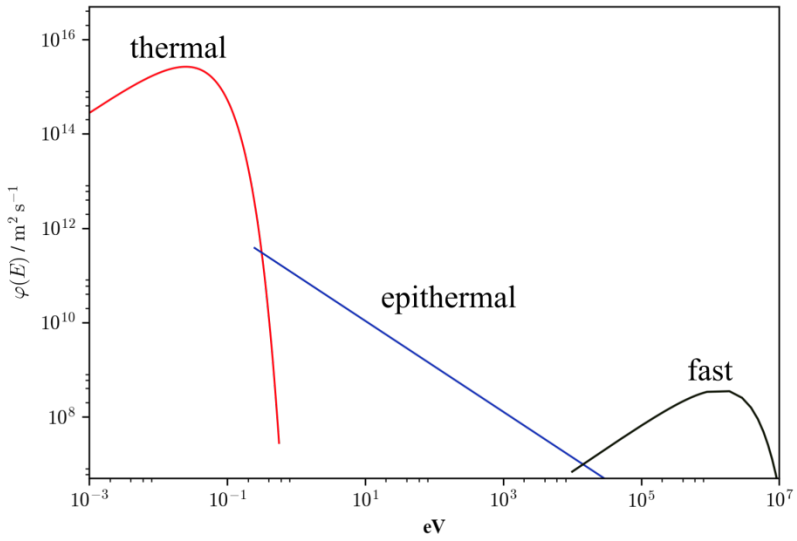

The σ value shows an inverse proportionality on neutron velocity in the whole energy range while in the epithermal region some resonances (zones with exceptionally high affinity for neutron absorption) are present. In addition, $n(v)$ has the shape of a maxwellian distribution in the thermal range, with maximum at the speed corresponding to neutron temperature, and inversely proportional in the epithermal range. Also the integral can be conveniently split in two parts (neglecting the fast region).

$$R = v_0\sigma_0 \int_0^{v_{Cd}} n(v)\,dv + \Phi_{epi} \int_{E_{Cd}}^\infty \frac{\sigma(E_n)\,dE_n}{E_n}, \tag{3}$$

where v_0 and σ_0 are velocity and cross section evaluated at a standard neutron velocity of 2200 m s^{-1}, that is the most probable speed at 20° C, corresponding to neutron energy of 0.0253 eV; integral of $n(v)$ is the thermal neutron density and its product with v_0 yields the conventional thermal neutron flux, Φ_{th}; Φ_{epi} is the conventional epithermal neutron flux and it can be seen as flux at the

neutron energy of exactly 1 eV and E_n represents the neutron energy. The integral in the second part of equation includes the cross section in the epithermal region and takes into account all the occurring resonances and is called resonance integral in the ideal flux, I_0. In a real neutron flux, since the behavior deviates from $1/E_n$, an epithermal flux distribution parameter, α, is added leading to the resonance integral in the real flux, $I_0(\alpha)$.

$$I_0(\alpha) = \int_{E_{Cd}}^{\infty} \frac{\sigma(E_n)\, dE_n}{E_n^{(1+\alpha)}}, \tag{4}$$

Conversion between I_0 and $I_0(\alpha)$ is possible when behavior of $\sigma(v)$ of target isotope is proportional to $1/v$ up to 1-2 eV:[18]

$$I_0(\alpha) = \frac{I_0 - 0.429\,\sigma_0}{\bar{E}_r^{\alpha}} + \frac{0.429\,\sigma_0}{(2\alpha+1)(E_{Cd})^{\alpha}}, \tag{5}$$

where $\bar{E}_r$ is the effective resonance energy representing a single virtual resonance energy acting as the total cross section of resonances.[19] Scalar 0.429 is the result of a ratio of defined energies: $0.429 = 2\sqrt{\frac{E_0}{E_{Cd}}}$, where E_0 is the most probable neutron energy (0.0253 eV) thus, eq. 5 is valid only in case E_{Cd} is 0.55 eV. Multiple conditions need to be encountered to satisfy the 0.55 eV assumption: $1/v$ dependence of target nuclide cross section, homogeneous and isotropic neutron flux and cylindrical shape of Cd-box with 1 mm thickness of walls and height/diameter ratio of 2.[20]

In Høgdahl convention, reaction rate per target nucleus can be simplified with sum of a thermal and an epithermal component:

$$R = \Phi_{th}\sigma_0 + \Phi_e I_0(\alpha), \tag{6}$$

or alternatively:

$$R = \Phi_{th}\sigma_0 \left(1 + \frac{Q_0(\alpha)}{f}\right), \tag{7}$$

where $Q_0(\alpha)$ is the resonance integral considering α correction to thermal (2200 m s^{-1}) cross section ratio and f is the thermal to epithermal conventional flux ratio.

Westcott formalism is an extension of the Høgdahl convention. The distinction in thermal and epithermal regions remains, in addition, a further parameter accounting for neutron temperature is added:

$$R = \Phi_{th}\sigma_0 \left(g(T_n) + r(\alpha)\sqrt{\frac{T_n}{T_0}}\, s_0(\alpha)\right), \tag{8}$$

where $g(T_n)$ is the Westcott factor, it depends on the neutron temperature and for non-$1/v$ nuclides (for those σ_{th} doesn't follow $1/v$ proportionality) it deviates from 1, $r(\alpha)\sqrt{\frac{T_n}{T_0}}$ is the modified spectral index, it replaces f^{-1} in the Høgdahl formulation and it corresponds to the epithermal to total neutron density ratio according to neutron temperature and should be experimentally evaluated,

$s_0(\alpha)$ is the modified reduced resonance integral for the real epithermal spectrum (including correction factor α) on 2200 m s^{-1} cross section.[21,22]

Høgdahl convention is only valid for target isotopes which $1/v$ σ dependence holds up to 1.5 eV. The most part of nuclides observes this behavior and for just a few isotopes (for example ^{151}Eu, ^{176}Lu, when activated with (n,γ) reaction) the convention is not applicable (Figure 3). However, the simplicity of its statements and reliability for most part of nuclides makes Høgdahl the main convention used in NAA.

Figure 3: Typical $1/v$ and non-$1/v$ cross sections are showed together. ^{151}Eu (non-$1/v$ behavior) highlights dramatic deviation from linearity in the range up to 1.5 eV.

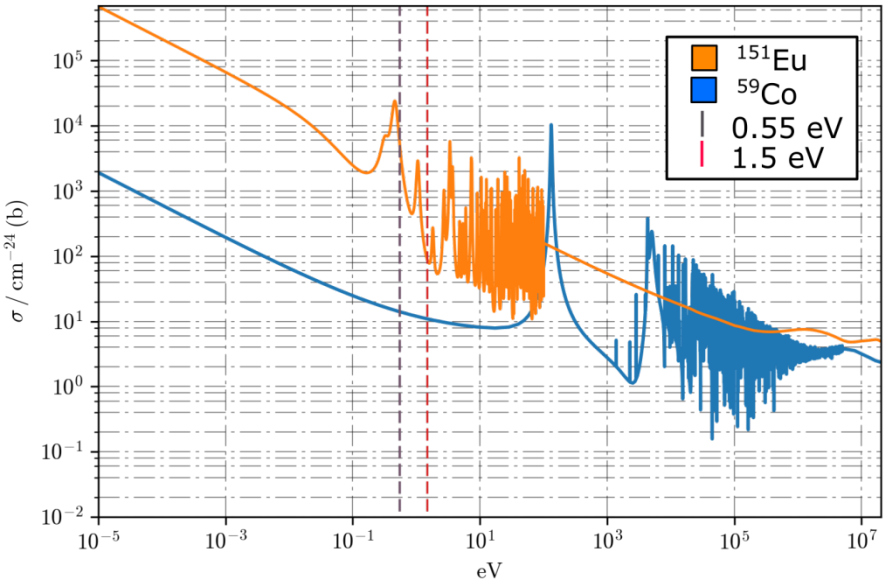

The amount of produced radionuclides at the end of neutron irradiation is modeled by a differential equation. In the simpler situation, starting amount of radionuclides that has to be produced is zero, then, activated isotopes are exclusively obtained by irradiation:

$$N(t_i) = \frac{R\,N_0}{\lambda}(1 - e^{-\lambda t_i}), \tag{9}$$

where $N(t_i)$ is the amount of radionuclides produced at time t_i, the end of irradiation, while N_0 is the initial amount of target isotope.

Decay of radionuclide that can occur between end of irradiation and start of spectrum acquisition is taken into account and N is corrected for by means of the radioactive decay formulae according to:

$$N(t_d) = \frac{R\,N_0}{\lambda}(1 - e^{-\lambda t_i})\,e^{-\lambda t_d}, \tag{10}$$

where $N(t_d)$ is the amount of radionuclides at time t_d, the time passed after the end of irradiation.

The number of radionuclides decayed during time of spectrum acquisition, $N(t_c)$, is:

$$N(t_c) = \frac{R\,N_0}{\lambda}\left(1 - e^{-\lambda t_i}\right) e^{-\lambda t_d}(1 - e^{-\lambda t_c}), \quad (11)$$

where t_c, is the acquisition time.

Signals recorded in the acquisition phase of a INAA protocol are generally γ-rays. Their amount is linked to the target nuclide:

$$n'_p = \frac{R\,N_0}{\lambda}\left(1 - e^{-\lambda t_i}\right) e^{-\lambda t_d}\left(1 - e^{-\lambda t_c}\right) \Gamma\,\varepsilon\,\frac{t_l}{t_c}, \quad (12)$$

where n'_p is the number of counts in the full-energy peak corrected for coincidence sums and losses, Γ is the gamma ray intensity, t_l is the live time, the effective time in which the system is actually acquiring incoming gammas and ε is the full-energy peak efficiency, i.e. the ratio between the number of emitted gammas from the source and the number of counts in the full-energy peak. It is worth noting that ε value depends on various parameters: geometrical factors (positions and volumes) related to solid angle between gamma source and detector and interactions of incoming gamma with detector that predict how many emissions directed towards the detector are able to interact with it and how much of the interacting amount of gamma is converted in signals corresponding to full-energy peak.

Il follows from eq. 12 the model linking the number of counts of full-energy peak and parameters carried out from nuclear databases and the number of the target isotope in the sample:

$$N_0 = \frac{n'_p\,\lambda\,t_c}{t_l\,R\left(1-e^{-\lambda t_i}\right) e^{-\lambda t_d}\left(1-e^{-\lambda t_c}\right)\Gamma\,\varepsilon}. \quad (13)$$

In some cases, characteristics of the sample have to be taken into account and correction factors should be added if necessary. In particular, parameters dealing with neutron self-shielding in phase of activation, G_{ss}, and gamma self-absorption in phase of counting, G_{sa}, cannot be neglected when a massive sample is analyzed or strong shielding (target isotopes with large σ) or absorbing (isotopes with high Z and density) materials are present. G_{ss} accounts for the decrease of neutron flux when absorber isotopes are encountered on the neutron path; it is composed of a thermal self-shielding factor and an epithermal self-shielding one.

Using the Høgdahl convention, the self-shielding factor can be expressed as follows:[23]

$$G_{ss} = \frac{G_{th} f}{f+Q_0(\alpha)} + \frac{G_e\,Q_0(\alpha)}{f+Q_0(\alpha)}, \quad (14)$$

where G_{th}, accounts for the neutron flux decrease in the thermal range while, G_e, accounts for the neutron flux decrease in the epithermal range. The G_e value is isotope dependent and depends on the resonance energies of that target.

Self-absorption depends on the interaction between gamma rays emitted by the radioactive source and electron rich isotopes. A general correction model for cylindrical shaped samples can be assimilated to a typical exponential attenuation trend:

$$K_{sa} = \frac{1}{\mu_l h}\left(1 - e^{-\mu_l h}\right), \quad (15)$$

where μ_l is the linear attenuation coefficient, i.e. the product between attenuation coefficient, μ, and density of sample, ρ, and h is the height of sample. The μ value is strongly energy dependent and reaches maximum levels for low-energy gamma-rays.

2.2 The ^{30}Si mole fraction

To assure continuity between units of old and new SI, values of the adopted natural constants should be evaluated with better, or at least similar, relative uncertainty fixed as a target for the new units. Concerning the unit of mass, the relative uncertainty target was within 2×10^{-8}; that means h and N_A values have to be measured within this target uncertainty.

Silicon has three natural occurring isotopes: ^{28}Si, ^{29}Si and ^{30}Si, the latter two representing the minor isotopes with a cumulate occurrence of approximately 7.4 % mole fraction[24]. Application of analytical techniques to assess molar mass on a material composed with naturally occurring Si isotopes is not trivial within the goal of 10^{-8} relative uncertainty. It is worth noting that M can be written excluding the dependence on mole fraction of ^{28}Si:

$$M = M(^{28}\mathrm{Si}) + x(^{29}\mathrm{Si})(M(^{29}\mathrm{Si}) - M(^{28}\mathrm{Si})) + x(^{30}\mathrm{Si})(M(^{30}\mathrm{Si}) - M(^{28}\mathrm{Si})). \quad (16)$$

This implies that combined uncertainty depends only on uncertainty on mole fractions of less abundant isotopes (uncertainties on isotopic molar masses are always orders of magnitude lower than mole fractions and can be considered negligible). Use of enriched ^{28}Si is mandatory to reach the target uncertainty: in fact, the lower amount a minor isotope is present the lesser strict measurement uncertainty is required to get the same combined uncertainty on M. An adequate analytical method suitable for trace elements investigation is however mandatory.

ICP-IDMS was extensively used for quantification of amount of substance fraction for ^{29}Si and ^{30}Si. In a particular case, a discrepancy observed among values obtained from different National Metrology Institutes (NMIs) using slightly different procedures pointed out a systematic error in one of the two approaches.[25] (Figure 4) In particular, the value obtained by National Research Council (NRC, Canada) seemed to be discrepant from the quantification performed by PTB, National Metrology Institute of Japan (NMIJ) and National Institute of Standard and Technology (NIST, USA).

Figure 4: Discrepancy observed among mole fractions results obtained with the highly enriched ^{28}Si in Avogadro materials. Analyses were all performed by NMIs with ICP-IDMS. NRC value is showed in the bottom left corner of the graph, uncertainty bars at k=2 coverage factor are represented.

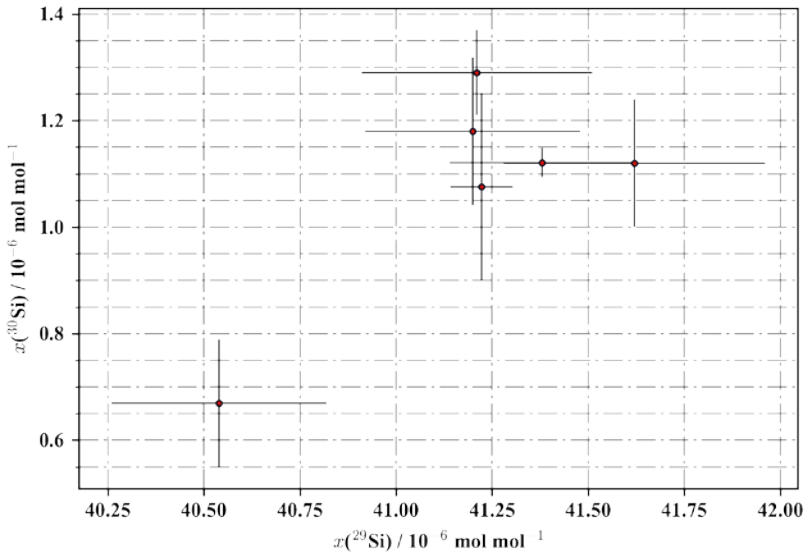

The adoption of an analytical method based on a completely different physical principle was useful to solve the controversy. Instrumental Neutron Activation Analysis (INAA) was used to determine the $x(^{30}\mathrm{Si})$ value.

Silicon is a perfect matrix for INAA analysis as activated radionuclides have very short half-life: ^{28}Al and ^{29}Al, main products formed from ^{28}Si and ^{29}Si via (n,p) reaction, show 2.245(2) min and 6.56(6) min half-lives, respectively, and ^{31}Si obtained from ^{30}Si via (n,γ) has 157.36(26) minutes half-life.[26,27] Here and hereafter the standard uncertainty, $k = 1$, indicated in parenthesis applies to the last respective digits. Side reactions can occur with formation of ^{24}Na and ^{28}Mg, which amount is determined by intensity and profile of neutron flux as they are formed by reactions promoted in the fast part of neutron spectrum. Nevertheless, they are produced in small quantity and don't affect analysis. The ^{30}Si value can be quite easily determined by taking advantage of the longer half-life of its product ^{31}Si. On the other hand, quantification of ^{29}Si in the enriched crystal would be impossible to assess with required accuracy. In fact, the extremely low amount of ^{29}Si and the short half-life of the produced ^{29}Al make it barely detectable with an INAA experiment. Anyway the quantification of ^{30}Si results in paramount information on the molar mass to confirm values obtained with IDMS.

The strategy proposed to measure the ^{30}Si mole fraction in highly enriched silicon samples consisted in a relative INAA analysis. This method compares the unknown sample with a standard; the adopted standard is another silicon sample manufactured with the same crystal growth process and of natural isotopic composition certified by a NMI. ^{30}Si mole fraction of unknown material is obtained from ratio of INAA measurement model applied to sample and standard. Advantages of relative method consist in the possibility to neglect many parameters thus simplifying the model. In detail, when sample and standard are co-irradiated, the production rate can be considered equal if neutron flux is constant. Otherwise, flux monitors can be used for appropriate radionuclide production correction. In addition, if samples have the same geometry and they are placed in identical position in phase of gamma counting, the ratio of efficiencies is considered extremely close to 1 as all the other correction parameters. The following measurement model applies,

$$x(^{30}\mathrm{Si_s}) = \kappa_{\mathrm{td}}\kappa_{\mathrm{R}}\kappa_{\varepsilon}\kappa_{\mathrm{ss}}\kappa_{\mathrm{sa}}\kappa_{\mathrm{g}}\frac{C_{\mathrm{s}}(t_{\mathrm{d}})}{C_{\mathrm{n}}(t_{\mathrm{d}})}x(^{30}\mathrm{Si_n})\frac{m_{\mathrm{n}}M_{\mathrm{s}}}{m_{\mathrm{s}}M_{\mathrm{n}}}, \tag{17}$$

where subscript s and n refer to highly enriched sample and natural standard sample, respectively. Parameters κ_{td}, κ_{R}, κ_{ε}, κ_{ss}, κ_{sa} and κ_{g} are the correction factors. $\kappa_{\mathrm{td}} = e^{-\lambda(\mathrm{td,n-td,s})}$, accounts for decay time between sample and standard;

$$\kappa_{\mathrm{R}} = K_{\mathrm{R\,m}}\,\frac{\left(1+\frac{Q_{0\,\mathrm{m}}(\alpha)}{f_{\mathrm{s}}}\right)\left(1+\frac{Q_0(\alpha)}{f_{\mathrm{n}}}\right)}{\left(1+\frac{Q_{0\,\mathrm{m}}(\alpha)}{f_{\mathrm{n}}}\right)\left(1+\frac{Q_0(\alpha)}{f_{\mathrm{s}}}\right)} \tag{18}$$

accounts for activation variation due to flux inhomogeneities; κ_{ε} accounts for detection efficiencies of sample and standard, κ_{ss} and κ_{sa} account for self-shielding and self-absorption of sample and standard, respectively; κ_{g} accounts for differences in geometrical shape between samples; $C(t_{\mathrm{d}})$ is the 1266.1 keV full-energy peak count rate at time t_{d} after irradiation end; $x(^{30}\mathrm{Si})$, m and M are the $^{30}\mathrm{Si}$ mole fraction, the mass and molar mass of sample, respectively. In detail in eq. 18,

$$K_{\mathrm{R\,m}} = \frac{1}{\kappa_{\mathrm{td\,m}}\kappa_{\varepsilon\,\mathrm{m}}\kappa_{\mathrm{ss\,m}}\kappa_{\mathrm{sa\,m}}\kappa_{\mathrm{g\,m}}}\frac{C_{\mathrm{m\text{-}n}}(\mathrm{td\ m\text{-}n})}{C_{\mathrm{m\text{-}s}}(\mathrm{td\ m\text{-}s})}\frac{m_{\mathrm{m\text{-}s}}}{m_{\mathrm{m\text{-}n}}}, \tag{19}$$

where m-n and m-s refer to monitors associated with natural sample and standard, respectively, with all parameters analogue to that present in eq. 17. Moroever, $C(t_{\mathrm{d}})$ can be stated by an average of following countings, reporting each obtained value of count rate to the decay time of the first acquisition, in order to reduce statistical uncertainty according to:

$$C(t_{\mathrm{d}}) = \frac{\lambda\, n_{\mathrm{c},i}\, t_{\mathrm{c},i}}{e^{-\lambda\left(t_{\mathrm{d},i}-t_{\mathrm{d}}\right)}\left(1-e^{-\lambda\, t_{\mathrm{c},i}}\right) t_{\mathrm{l},i}}, \tag{20}$$

where subscript i refers to the i^{th} acquisition and t_{d} to the reference decay time.

This model was successfully applied to test the feasibility of the application of INAA method for $x(^{30}\mathrm{Si})$ assessment on Avogadro crystals[28]. In the mentioned case, quantification of about 1×10^{-6} mol mol^{-1} of $^{30}\mathrm{Si}$ from an official silicon sample enriched in isotope 28 was reached with 1.8% uncertainty, that means within the required target.

However, another measurement model is obtained from eq. 17 to calculate $x(^{30}\mathrm{Si})$ in case the co-irradiation cannot be performed or sample and standard have to be irradiated in the same channel but for different irradiation times. The role of flux monitor is even more decisive for the correction of different irradiation times and possible non homogeneities of the average flux during irradiations.

A drawback in comparison to the co-irradiation procedure consists in the expected larger uncertainty of $x(^{30}\mathrm{Si})$ due to the different irradiation times. On the other hand, the possibility to independently adjust the neutron exposure of sample and standard has the advantage of reducing the difference in decay times and consequently the uncertainty of κ_{td}. The following measurement model applies:

$$x(^{30}\mathrm{Si_s}) = \kappa_{\mathrm{ti}}\kappa_{\mathrm{td}}\kappa_{\mathrm{R}}\kappa_{\varepsilon}\kappa_{\mathrm{ss}}\kappa_{\mathrm{sa}}\kappa_{\mathrm{g}}\frac{C_{\mathrm{s}}(t_{\mathrm{d}})}{C_{\mathrm{n}}(t_{\mathrm{d}})}x(^{30}\mathrm{Si_n})\frac{m_{\mathrm{n}}M_{\mathrm{s}}}{m_{\mathrm{s}}M_{\mathrm{n}}}, \tag{21}$$

where $\kappa_{ti} = \frac{\left(1-e^{-\lambda t_{i,n}}\right)}{\left(1-e^{-\lambda t_{i,s}}\right)}$ is the correction factor due to different irradiation times of sample and standard. Likewise, an equivalent correction factor for irradiation time of the monitors, $\kappa_{ti\ m}$, appears in $K_{R\ m}$ (eq. 19) alongside the other correction factors.

Another improvement to slightly reduce combined uncertainty consisted in a new determination of $t_{1/2}$ of ^{31}Si as its presently adopted value, a weighted average calculated from 10 measurements performed between 1937 and 1993, was not revised since very long time; moreover, the analysis of the published papers showed in some case an incomplete or unsatisfactory uncertainty statement. The measurement was performed through several observations of 1266 keV γ-emission from the exponential decay of ^{31}Si produced in a silicon sample during neutron irradiation.[29]

2.3 Bulk contamination

Apart from a few light elements (B, C, N, O, P) measured with infrared spectrometry[30], the absence of possible elemental impurities in the bulk of silicon crystal was assumed but not experimentally verified. Presence of any element, different from Si, in interstitial or substitutional sites should be considered accordingly to correct the weighted mass of the silicon sphere. INAA can fit well the task to quantify a wide range of isotopes present in ultra-trace amounts in a Si matrix.[31] However, applicability of relative method in this kind of situation is rather cumbersome, due to the critical aspect of multiple standard preparation. Thus, the possibility, offered by k_0-INAA standardization method, to quantify the most part of elements present in the periodic table using a comparator element represents a surprising step ahead for the characterization of this particular Si materials.

Precursor of k_0 was the single comparator method proposed by Girardi;[32] his procedure derived from the consideration that after irradiation of known quantities of an element of interest with a comparator element, that can be of course different from the first one, and following gamma acquisition with determined positions, it is possible to quantify a constant, k, that links the two elements.

$$k_c(s) = \frac{\left|\frac{n'_p\,\lambda\,t_c}{\left(1-e^{-\lambda t_i}\right)e^{-\lambda t_d}\left(1-e^{-\lambda t_c}\right)t_c\,m}\right|_s}{\left|\frac{n'_p\,\lambda\,t_c}{\left(1-e^{-\lambda t_i}\right)e^{-\lambda t_d}\left(1-e^{-\lambda t_c}\right)t_c\,m}\right|_c}, \qquad (22)$$

where subscripts c and s indicates comparator and element of interest, respectively. The knowledge of $k_c(s)$ allows to quantify unknown amount of element of interest in a sample with INAA if, during actual analysis, most part of experimental conditions (channel of irradiation and flux, detector, position and geometry of acquisition) remains unaltered from $k_c(s)$ evaluation.

Measured $k_c(s)$ factors give the possibility to quantify a great number of elements using a single comparator. However, the main drawback of the method consists in the limitation due to tight

dependence on local variables; in case of any modification of the protocol, e.g. irradiation channel or acquisition geometry, measured $k_c(s)$ factors must be re-determined.

In order to overcome the problem, single comparator method was modified and $k_c(s)$ factors expressed in a constant and a variable part:

$$k_c(s) = \frac{M_c \theta_s \Gamma_s \sigma_{0,s}}{M_s \theta_c \Gamma_c \sigma_{0,c}} \frac{G_{th,s} f + G_{e,s} Q_{0,s}(\alpha)}{G_{th,c} f + G_{e,c} Q_{0,c}(\alpha)} \frac{\varepsilon_s}{\varepsilon_c}, \tag{23}$$

where M is the molar mass and θ is the isotopic abundance; together with Γ and σ_0 they compose the constant portion of $k_c(s)$ and are condensed in a new parameter, $k_{0,c}(s)$. Obtained k_0 parameter is independent from experimental variables and can be used in every laboratory. To reach international standardization, 411.8 keV gamma line deriving from activation of ^{197}Au was designated as the ultimate comparator and a database was issued including $k_{0,Au}(s)$ values. The $k_{0,Au}$ value of an element is a very useful parameter, in fact it allows to choose any kind of comparator among the elements present in the database, as k_0 factor of an element referred to a specific comparator can be easily obtained from the combination of the two relative $k_{0,Au}$; in detail, $k_{0,c}(s) = \frac{k_{0,Au}(s)}{k_{0,Au}(c)}$. The latest release of k_0 database[33], issued at the end of 2015, consists of more than 440 recorded gamma lines for sixty-seven elements allowing extensive multi-elemental analysis.

The mass fraction of every element of interest, s, in the investigated sample, and listed in the k_0 database, can be quantified with a single co-irradiated comparator according to:[20]

$$\rho_s = \frac{\left| \frac{n_p' \lambda t_c}{\left(1-e^{-\lambda t_i}\right) e^{-\lambda t_d} \left(1-e^{-\lambda t_c}\right) t_c w} \right|_s}{\left| \frac{n_p' \lambda t_c}{\left(1-e^{-\lambda t_i}\right) e^{-\lambda t_d} \left(1-e^{-\lambda t_c}\right) t_c m} \right|_c} \frac{k_{0,Au}(c)}{k_{0,Au}(s)} \frac{G_{th,c} f + G_{e,c} Q_{0,c}(\alpha)}{G_{th,s} f + G_{e,s} Q_{0,s}(\alpha)} \frac{\varepsilon_c}{\varepsilon_s}, \tag{24}$$

where ρ_s is the mass fraction of analyte s referred to the mass of investigated sample indicated with w, in order to distinguish it from m that represents the actual mass of the comparator element, only. All other parameters have already been discussed.

The measurement model showed in eq. 24 assumes that flux parameters remain constant during the whole irradiation time and elements of comparator and sample have naturally occurring isotopic abundance, as $k_{0,Au}$ values are experimentally determined using material with natural isotopic abundance. Moreover, it refers to neutron flux according to the Høgdahl convention. For non-1/v nuclides Westcott formalism must be introduced. The measurement model becomes:

$$\rho_s = \frac{\left| \frac{n_p' \lambda t_c}{\left(1-e^{-\lambda t_i}\right) e^{-\lambda t_d} \left(1-e^{-\lambda t_c}\right) t_c w} \right|_s}{\left| \frac{n_p' \lambda t_c}{\left(1-e^{-\lambda t_i}\right) e^{-\lambda t_d} \left(1-e^{-\lambda t_c}\right) t_c m} \right|_c} \frac{k_{0,Au}(c)}{k_{0,Au}(s)} \frac{G_{th,c}\, g(T_n) + G_{r,c}\, r(\alpha) \sqrt{\frac{T_n}{T_0}}\, s_{0,c}(\alpha)}{G_{th,s}\, g(T_n) + G_{r,s}\, r(\alpha) \sqrt{\frac{T_n}{T_0}}\, s_{0,s}(\alpha)} \frac{\varepsilon_c}{\varepsilon_s}, \tag{25}$$

where G_r is the resonance self-shielding correction factor that can be converted to the already known epithermal self-shielding, G_e according to: $G_r = G_e - \epsilon(1 - G_e)$, where ϵ is the fraction of 1/v (underlying resonances) to the epithermal component of activation.

An experiment based on k_0-NAA method was performed on a sample of the highly enriched silicon crystal used to determine N_A to examine the widest range of possible contaminant elements and find out the total amount of impurities. A detection limit was issued, instead, as an upper limit for elements present in such a small quantity that could not be detected. In order to extend the investigation through the largest possible number of elements, a short and a long irradiation were consecutively performed.

2.4 Vacancies concentration

Latest aim related to the characterization of enriched silicon materials for redetermination of Avogadro constant involved the quantification of vacancies. Vacancies affect the mass of the silicon spheres like the impurities. Analogously for what concerned $x(^{30}Si)$ measurement, this kind of investigation on highly enriched Si materials was just performed by a single analytical method, i.e. positron annihilation lifetime spectroscopy (LPS).[34] Also in this case, the development and application of an independent measurement method can be advantageous to complete the piece of information given by LPS. In fact, only small aggregates, up to a few vacancies, are likely to be detected by LPS while aggregates forming voids up to 30 nm diameter remained uncovered. Presence of voids over 30 nm diameter was instead excluded by analysis performed with laser scattering tomography (LST).

The analytical procedure proposed to estimate the vacancies concentration is based on the Cu diffusion method[35] coupled with INAA as a means of Cu detection. In detail, this method exploits the extremely high diffusivity of metals in Si, and especially of Cu among them. The elevated Cu diffusion coefficient, due to the presence of interstitial atoms that are free to move in Si, is proportional to temperature; then, if a Cu layer is applied on Si external surface and high temperature is provided, Cu can diffuse towards the internal portion of crystal at a speed of centimeters in a few hours at about 800 K. Part of the Cu inside the Si crystal forms a thin film on the internal cavity walls due to their high affinity. If temperature is slowly decreased and copper external layer is still at his place, super-saturation of Cu in Si becomes the driving force for the precipitation of copper silicide, Cu_3Si, within the cavities. At this point, etching is needed in order to clean the external Cu layer and a cycle of further annealings at lower temperature, followed by etchings is necessary to allow the complete exit of un-precipitated interstitial Cu. When no more Cu can be subtracted from crystal only the precipitated Cu_3Si trapped in voids remains at its place.

From the quantification of copper and knowledge of molar volume of Cu_3Si it is possible to retrieve the void volume within the examined crystal and, consequently, the vacancies concentration. The analytical method proposed in the original procedure to assess Cu amount was mass spectrometry. However, with mass spectrometry, dissolution of sample is mandatory; for that reason the procedure of in- and out- diffusion should be performed in different similar crystals to monitor the level of Cu. Instead, INAA was suggested to allow Cu quantification at every step of the annealing protocol on the same Si crystal. The high sensibility of INAA method makes it able to detect the

estimated target amount of copper; moreover, the possibility to prevent digestion of such a valuable sample is always a great advantage. The relative standardization method was adopted.

The measurement model is similar to that applied for $x(^{30}\mathrm{Si})$ quantification in case of co-irradiation (eq. 17). In this case, the measurand is the number density of Cu, N_{Cu}, assuming natural isotopic abundance:

$$N_{\mathrm{Cu}} = \kappa_{\mathrm{td}}\kappa_{\mathrm{R}}\kappa_{\varepsilon}\kappa_{\mathrm{ss}}\kappa_{\mathrm{sa}}\kappa_{\mathrm{g}}\frac{\mathrm{C_s}(t_{\mathrm{d}})}{\mathrm{C_n}(t_{\mathrm{d}})}\frac{m_{\mathrm{n}}N_{\mathrm{A}}d_{\mathrm{s}}}{m_{\mathrm{s}}M_{\mathrm{n}}}, \tag{26}$$

where subscripts s and n refer to the Si sample and Cu standard, respectively and *d* is the density of natural silicon.

The vacancies concentration, i.e. the number of vacancies per unit of silicon volume, N_{v}, is straightforwardly obtained according to:

$$N_{\mathrm{v}} = \frac{N_{\mathrm{Cu}}}{3\,V_{\mathrm{m\,Si}}}\left(V_{\mathrm{m\,Cu_3Si}} - V_{\mathrm{m\,Si}}\right), \tag{27}$$

where V_{m} are the molar volumes of η' phase of precipitated Cu_3Si and Si. The N_{v} value corresponds to the vacancies concentration under the assumption that all the voids are completely filled with Cu_3Si and interstitial Cu is completely out-diffused. The N_{v} value is likely to be considered as an upper limit because of the possibility that other defects can also act as precipitation sites for Cu_3Si; for example, Cu_3Si precipitate itself introduces stress in the lattice inducing further voids formation. However, estimate of vacancies concentration carries important information revealing whether point defect correction may be required or not on the highly ^{28}Si-enriched silicon crystals for Avogadro redetermination.

3. Experimental

3.1 The ^{30}Si mole fraction

A sample of the latest manufactured highly enriched silicon mono-crystal[36] was used to measure the mole fraction of ^{30}Si. Based on the existing data, the $x(^{30}\mathrm{Si})$ value is expected to be lesser than 1×10^{-6} mol mol^{-1}. The sample was cut by PTB from one of the produced batches and identified with code Si28−23Pr11 part Q.4.1. Sample had perfect shape of a small cylinder of about 6.0 cm^3 volume with 20.07 mm diameter of and 19.06 mm height and about 14 g mass. (Figure 5)

Figure 5: Picture of investigated ^{28}Si enriched sample.

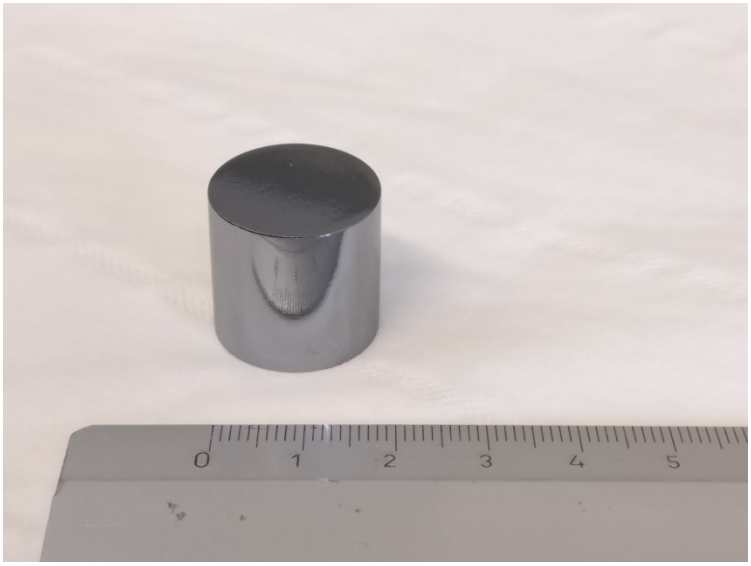

Another silicon single crystal, produced with the same float zone technique and cut in the same cylindrical shape, was used as the standard for ^{30}Si quantification. Dimensions of the standard were as similar as possible to the dimensions of the enriched sample and corresponded to 20.05 mm diameter and 19.07 mm height. The natural isotopic abundance of Si was evaluated by PTB with mass spectrometry. The analysis yielded a $x(^{30}\mathrm{Si})$ value of 0.031031(48) mol mol^{-1} and a molar mass value of 28.08570(21) g mol^{-1}.

Sample and standard were deeply etched as they were received from PTB in order to remove the external contamination due to machining, storage and transportation. Etching procedure included a series of washings in organic and inorganic solutions that were in sequence: (i) trichloroethylene (C_2HCl_3), (ii) acetone (C_3H_6O), (iii) deionized water, (iv) concentrated nitric and hydrofluoric acids in 10:1 volume proportion (HNO_3:HF), (v) deionized water, (vi) acetone. Great care was applied to avoid cross-contamination of ^{30}Si between samples during all the etching phases. To this aim, enriched sample was always handled first. After etching, samples were weighed using a digital analytical balance calibrated with SI-traceable weights; resulting masses yielded 13.5073(1) g for ^{28}Si enriched crystal and 13.5496(1) g for the natural one.

Two samples, about 70 mm length, of an Al-Co wire (IRMM-527RB, 0.1% Co mass fraction, 0.5 mm diameter) were used as flux monitors. Their masses, measured on an high precision analytical balance calibrated with SI-traceable weights, were 0.03395(1) g and 0.04104(1) g for wire associated with enriched and natural crystal, respectively.

Each silicon crystal was wrapped in an ultrapure Al foil and surrounded by a single helix of the assigned Al-Co wire. Then, a second Al foil was used to tightly envelop the sample and keep the monitor in its position. Enriched and natural sample, each one embraced by the respective monitor, were closed in different containers ready for neutron irradiation.

Irradiation took place in the OPAL reactor managed by Australian Nuclear science and Technology Organisation (ANSTO) situated in Sydney. OPAL is a 20 MW open pool reactor fueled with low enriched uranium (fissile ^{235}U mass fraction < 20%) and moderated using both light and heavy

water (light water in the primary coolant, then heavy water lies in the reflector between the core and irradiation positions). Irradiation channel named LE7−1C (Φ_{th} = 1.0 × 10^{14} cm^{-2} s^{-1}, f = 44.3) was preferred for the analysis due to the extremely high neutron flux, more than 1 order of magnitude compared to flux where preliminary feasibility tests were performed[28,37], despite flux thermalization, indicated by f value, was worse than other irradiation facilities of OPAL. Samples were irradiated separately with one week delay. Also irradiation times were different to compensate the difference of about 5 orders of magnitude in ^{30}Si amount between the two samples; ^{28}Si enriched was irradiated first for 10800(17) s while natural crystal was irradiated later for 3600(17) s. Albeit one week can be considered a great delay to perform this kind of analysis, the online measurement of the neutron flux fluctuation during each irradiation showed no significant departures from the mean value of the previously fixed set point.

After irradiation, the Al foils fixing the monitor and surrounding the sample were removed. Each monitor wire was bent in a ring shape of 1 cm diameter to obtain a compact source geometry and was located in a polyethylene vial for counting.

Counting of 1266.1 keV γ-emission of radioisotope ^{31}Si was performed on a HPGe detector GMX50-P4 (70 mm crystal diameter, 65% relative efficiency, 1.87 keV full width at half maximum (FWHM) resolution at 1332 keV) from ORTEC connected to a digital signal processor ORTEC DSPEC-Pro. Enriched and natural sample were directly placed in contact to detector end-cap, with axis of the sample parallel to the axis of the Ge crystal, on a paper template corresponding to the center position. Afterwards, a series of spectra were acquired. The counting of the enriched started 286.9 min after the end of irradiation and consisted of a sequence of 3 spectra acquired consecutively fixing real time to 7200 s. The counting of the natural crystal started after 2284.0 min and consisted of 7 spectra acquired fixing real time to 4000 s. In both cases detection dead times were not higher than 18%, even in the worst cases, and did not represent a critical situation for detection system. Between the two series of acquisition, stability of energy calibration over time was checked by monitoring 1460.8 keV gamma peak from natural ^{40}K.

Counting of 1332.5 keV γ-emission of radioisotope ^{60}Co from flux monitors was performed on a different HPGe detector named GEM25-P4 (57 mm crystal diameter, 25% relative efficiency, 1.66 keV FWHM resolution at 1332 keV) from ORTEC that was connected to a different digital signal processor but of the same type of that used with GMX50-P4 detector. Vials containing the Al-Co wires were placed on a shelf fixed at a distance of 22 cm from detector end-cap in a manner that axis of the ring wire was parallel to the axis of the Ge crystal. Three spectra, were acquired for both flux monitors to check their repeatability. The acquisition of the monitor flux co-irradiated with the enriched silicon sample, started 1412.5 min after the end of the irradiation, each spectrum lasted 65, 72 and 150 min, respectively. The acquisition of the monitor flux co-irradiated with the natural sample, started 2879.5 min after irradiation and spectra lasted 140, 278, and 265 min. Dead time of monitor acquisitions was corrected online using the Zero Dead-Time mode implemented in the DSPEC-Pro.

Net counts of full energy peaks from 1266.1 keV ^{31}Si and 1332.5 keV ^{60}Co gamma emissions were evaluated using the Gaussian fit included in the regular peaks and moderate count rate algorithm of the software HyperLab. The contribution to the uncertainty due to statistics was also evaluated.

The full-energy peak count rate, $C(t_d)$, for enriched and natural samples and respective monitors, was extrapolated at t_d. A $C(t_d)$ value was calculated from each acquired spectrum of the same sequence and a weighted average was then performed with the aim to reduce statistical uncertainty that represented the main contributor to $C(t_d)$. Counting times, t_c and t_l, were retrieved from the spectrum information with negligible uncertainty. The ^{31}Si and ^{60}Co decay constants, λ, were calculated using $t_{1/2}(^{31}\mathrm{Si}) = 157.23(16)$ min and $t_{1/2}(^{60}\mathrm{Co}) = 462.067(34) \times 10^2$ h.

The adopted $t_{1/2}(^{31}\mathrm{Si})$ value was the weighted average of the literature value[27] 157.36(26) min and a recent estimate[29], 157.16(20) min.

Mole fraction of ^{30}Si, $x(^{30}\mathrm{Si_n})$, together with molar mass, M_n, in the natural crystal were assessed through mass spectrometry by PTB.

Molar mass of enriched crystal, M_s, also appears in the measurement model (eq. 18). This may seem a paradox as one of the input parameters directly relies on the result of the analysis. However, the extremely high enrichment in ^{28}Si of the sample makes it unaffected from minor isotopes (^{29}Si and ^{30}Si) present in trace amounts. Value of M_s was thus assumed as the molar mass of ^{28}Si with the component due to sum of minor isotopes as the variability on M_s. Since the expected $x(^{29}\mathrm{Si})$ and $x(^{30}\mathrm{Si})$ values were 5×10^{-6} mol mol^{-1} and 0.7×10^{-6} mol mol^{-1}, M_s was evaluated as 27.976933 g mol^{-1} and assuming a uniform probability distribution within the interval $\pm 6.4 \times 10^{-6}$ g mol^{-1}; thus, corresponding to $M_s = 27.976933(4)$ g mol^{-1}.

Masses of two samples were weighed on analytical balance calibrated with weights traceable to SI after the end of sequences of acquisition.

Irradiation times, t_i, were recorded by the reactor management software running at the OPAL facility. Sample were pneumatically inserted and extracted but time resolution of the system was not better than 1 min and uncertainty was evaluated as an homogeneous distribution. Accordingly, irradiation times were evaluated as 10800(17) s and 3600(17) s for enriched sample and natural crystal respectively, both with relative flux monitor. t_i was required for κ_{ti} and $\kappa_{ti\ m}$ (part of κ_R) correction factors, in both case their value corresponded to 0.333(2).

Decay correction factor, κ_{td}, was evaluated by subtraction of decay times for sample, taken as reference, and standard, it resulted in a delay time of 1997 min with negligible uncertainty corresponding to a value of κ_{td} equal to $1.502(13) \times 10^{-4}$. Analogous decay correction factor concerning flux monitors was evaluated with the same method, in this case the resulting $\kappa_{td\ m}$ was 0.9996 with negligible uncertainty.

For efficiency correction parameter, κ_ε, the reproducibility of the vertical position with respect to the detector end-cap was taken into account, the main contribution to the detection efficiency resulted to be the height of the samples; in particular a difference between samples' height of 12 µm

(considering masses, densities and geometrical assumptions of perfect shape with same diameter) a variation in efficiency was assumed within ± 0.54% homogeneous. Accordingly, κ_{ε} = 1.000(3). $\kappa_{\varepsilon\ m}$ was instead assumed, due to the very large sample detector separation, to be exactly 1 with negligible uncertainty.

The effect of neutron self-shielding, κ_{ss}, was evaluated according to the model describing the sigmoid trend of self-shielding factors, G_{th} and G_e, against concentration of absorbing material.[38,39] Then, eq. 14 was applied to the two samples to get the corresponding κ_{ss} = 0.9944 within ± 2×10^{-4} as 4% of the estimated correction was assumed as the half-width of an homogeneous variability; thus κ_{ss} = 0.9944(1). Self-shielding correction factor affecting monitors, $\kappa_{ss\ m}$, was assumed 1 with negligible uncertainty.

Correction factors concerning self-absorption for samples and monitors, κ_{sa} and $\kappa_{sa\ m}$, were assumed to be negligible due to the quasi identical matrixes in the two cases; in addition, self-absorption of such high-energy gamma rays in silicon matrixes is scarce. However in the first case 0.01% standard uncertainty was assigned as a conservative approach, thus κ_{sa} = 1.0000(1).

Geometry correction factors, κ_g and $\kappa_{g\ m}$, were considered 1, due to the very similar geometry; also in this case, 0.01% standard uncertainty was attributed to the correction factor for samples.

Flux correction factor, κ_R was calculated through application of eq. 19 according to the experimental conditions, irradiation channel parameters and literature data. The adopted Q_0 values for ^{30}Si and ^{59}Co were 1.11(7) and 1.99(6), respectively.[33] Thus, κ_R = 1.0281(58), under the conservative assumption of ± 20% relative variation of f ($f_s = (1 \pm 0.2)\ f_n$ with the nominal f value: f_n = 44.3); the main contributor to the uncertainty resulted the $k_{ti\ m}$ parameter.

3.2 Bulk contamination

The measurement of the elemental contamination of the highly ^{28}Si enriched material used for the redetermination of the Avogadro constant was performed with INAA. The analysis concerned more than sixty elements and was carried out on the same sample used for $x(^{30}Si)$ evaluation.

Since a feasibility test, previously performed, highlighted the possibility to check the presence up to sixty-six elements,[40] also in this study the same k_0-NAA protocol was applied to the investigated sample to maximize the number of spotted analytes.

The sample Si28−23Pr11 part Q.4.1, was exposed to two different irradiations, a short one and a long one, in two channels of OPAL reactor.

For the short irradiation Au was chosen as the comparator due to the adequate half-life (2.7 days) of the main activation product, ^{198}Au: three samples, 2 mm length with 4 mg mass, of Al-Au wire (IRMM-530R, 0.1% mass fraction, 1 mm diameter) were used as mono-elemental standards for the application of k_0-method.

Enriched silicon sample was inserted in a 10 mL vial while Al-Au wires were located on the outer surface of vial at 120° with respect to the axis and fixed with adhesive tape. The short irradiation was performed in the NAA-SRT facility (nominal thermal neutron flux, Φ_{th} = 2.2 × 10^{13} cm^{-2} s^{-1}, with extremely high thermal to epithermal neutron flux ratio, f = 3250, α = 0.15 and provided with pneumatic system) for 300.0(6) s. At the end of irradiation, the crystal was moved from the vial and etched with HNO_3:HF 10:1 for 8 minutes, obtaining a mass of 13.5099(1) g with a loss of thickness in the order of few μm.

The γ-spectrometry measurements of the silicon sample were performed using a HPGe detector GEM35-70-PL (58 mm crystal diameter, 39% relative efficiency, 1.69 keV FWHM resolution at 1332 keV) from ORTEC. It was placed inside a low-background graded lead shield. The sample was located with its axis parallel to the axis of detector in central position and as close as possible (i.e. at about 10 mm) to the end-cap of the detector. Two spectra were sequentially collected after the short irradiation and etching; the first acquisition started 5263 s after the irradiation end and lasted 8088.5 s with negligible uncertainty and dead time, the second one started after 13501 s and lasted 63950.8 s.

The 411.8 keV emission of the Au comparators in three Al-Au wires was measured with an ORTEC GEM25P4-PLUS (59 mm crystal diameter, 32% relative efficiency, 1.67 keV FWHM resolution at 1332 keV) bent at the bottom of plastic counting vials at a distance of 21.6 cm from detector end-cap. The detectors were connected to ORTEC DSPEC-Pro digital spectrometers, and the data were collected using a personal computer running the ORTEC Maestro software. A single spectrum for each wire was acquired starting 3.5 h, 5.2 h and 21.4 h from the irradiation end and lasting 6070.8 s, 7318.8 s and 7299.9 s with negligible dead time, respectively.

The area of the full-energy peak or the corresponding background counts related to a detection limit according to the Currie's method[41], if peak was not present, were evaluated from the recorded spectra using the Hyperlab software to obtain value of n_p. In order to obtain n_p', correction for true coincidences effect was calculated using the SOLCOI routine of Kayzero for Windows software that exploited solid angle and coincidence correction computation using Monte Carlo approach.

Information about (n,γ) reactions, half-lives of related radionuclides, natural isotopic abundance of target nuclide, resonance integral to 2200 m s^{-1} cross section ratio and resonance energy parameters, Q_0 and $\bar{E}_r$, and gamma emissions were all retrieved from the k_0-database.[33]

Flux parameters of NAA-SRT channel were regularly checked.

Energy and efficiency calibration were obtained using certified standard sources and constantly checked. An efficiency fit was performed and the result recorded for each determined counting position relative to every detector. Detection efficiencies at different distances were calculated using the SOLCOI routine. Fine knowledge of detector physical parameters was required.

Investigation on long half-lives involved the same sample but the comparator consisted in a 70 mm length and 38 mg mass Al-Co wire (IRMM-527R, 0.1% Co mass fraction and 0.5 mm diameter). Silicon crystal was enveloped in a high purity Al foil (Sigma-Aldrich 356859, 99.8% Al mass

fraction and 50 μm thickness) with Co wire embraced to Al covered sample to form 1 turn of helix. Finally, a second Al foil was tightly enveloped in order to maintain the comparator in its position during irradiation container.

The long irradiation took place in the LE6-1C channel (f = 262.6, α = 0.14) and lasted 116.869(5) h.

After irradiation, the sample was slightly etched with HNO_3 and HF and placed on the GEM35-70-PL detector with its axis parallel to the axis of detector in central position and as close as possible (i.e. at about 10 mm) to the end-cap. Two spectra were collected in two gamma acquisitions lasting 88328.4 s and 156868.2 s with negligible dead time, respectively. However, as signals of Co, Ni and Fe due to possible external contamination from stainless steel appeared on those spectra, another, deeper, etching of the sample was performed. Loss of mass corresponded to more than 0.350 g from a starting mass of 13.4818 g. Successively, additional four spectra were acquired in four gamma acquisitions lasting 90720.2 s, 408998.4 s, 1015012.6 s and 870720.4 s, respectively. The absence of Ni and Fe signals in the recorded spectra, after deep etching, confirmed the removal of external contamination.

The mass fraction of a contaminant element present in the silicon sample, ρ_s, was obtained with calculations performed by Kayzero for Windows software based on eq. 24. In the case of a non-quantified element, when more than one detection limit was available, the lowest one was taken as the ultimate result. Counting statistics was, in general, the main contributor to the combined uncertainty of the results. In addition, a ±1 mm positioning tolerance of the silicon sample was assigned and gave a contribution of about 4% to the combined relative uncertainty. Mass fraction values, were given under the reasonable assumption of natural isotopic abundance of the impurities. Three analytes (Eu, Yb, Lu) didn't follow the 1/v dependence of σ_{th} in the range up to 1.5 eV and approximation of Høgdahl convention was not valid. Just for these elements, k_0-measurement model according to the Westcott formalism was adopted (eq. 25). Westcott $g(T_n)$ factors at 303 K (usual temperature reached during an irradiation in the used channels) for elements of interest were retrieved from literature[42] while $r(\alpha)\sqrt{\frac{T_n}{T_0}}$ parameter was previously experimentally evaluated in the LE6-1C irradiation channel. Finally, literature s_0 values were used for non-1/v nuclides and converted in $s_0(\alpha)$ values.

3.3 Vacancies concentration

The feasibility of application of Spaepen's Cu decoration method using INAA as the analytical technique was tested on a pure silicon single crystal of natural isotopic abundance. The sample had parallelepiped shape with squared base of 1 cm side and 5 cm height, corresponded to a volume of 5 cm^3. Mass of the crystal was 10.5 g.

The sample surface was cleaned by repeated cycles of Cu deposition by galvanic displacement with a water solution of $Cu(NO_3)_2$, and NH_4F. Thus, subsequent etching with a water solution of $FeCl_3$

was performed. When the Cu deposition, about 0.5 μm thick, looked regular and without visible defects, it was left as the Cu source and capping layer.

Cu diffusion phase was forced by heating up to 740 °C with an electrical oven in vacuum. The temperature was slowly increased starting from room temperature; then, the temperature of the oven was kept stable between 700 °C and 740 °C for about 3 h. After that period, the oven was switched off and the sample left in it to ensure the Cu_3Si precipitation into the voids due to the super-saturation occurring during the slow cooling rate (<3 °C min^{-1} in the worst case at the beginning of cooling, it took more than 10 h to return at room temperature).

Finally, the external Cu capping layer was removed by etching the sample with the HNO_3:HF solution for 40 min until external Cu was completely removed. The mass removed by etching, 485 mg, corresponded to a surface Si layer about 100 μm thick.

From that point, a cycle of out-diffusion of un-precipitated Cu by annealing and consecutive measurement of Cu amount at each step through Neutron Activation and gamma spectrometry was performed.

Out-diffusion was obtained by annealing the sample at 450 °C in air for 2 h; according to the protocol, the cooling rate was always less than 3 °C min^{-1}. Afterwards, the possible presence of Cu drained to the surface was eliminated by etching the sample with HNO_3:HF for 3 min. This slight removal corresponded to about 15 μm thickness lost by the sample.

Cu amount at each step of in- and out-diffusion was assessed with INAA-relative method. A copper wire ((Sigma-Aldrich, 99.999% Cu mass fraction, 0.1 mm diameter) cut with the same height of sample was used as standard. Silicon sample, and standard wire alongside it enveloped in a plastic shell, were irradiated in the TRIGA Mark II reactor situated in Pavia. Central channel was designated for neutron activation. TRIGA Mark II is a 250 kW pool type facility fueled with low enriched uranium and moderated with light water, its Central Channel is situated exactly at the center of the core and provides the position with major flux, $\Phi_{th} = 6.11(16) \times 10^{12}$ cm^{-2} s^{-1}, but not a high thermalization, $f = 15.6(3)$.[43] The irradiation lasted 360 min. After a dozen hours of decay, the silicon crystal was etched for 2 min to avoid any possible contamination during handling.

Gamma spectrometry measured the ^{64}Cu gamma peak at 1345.8 keV, emitted from silicon sample and standard. The acquisitions were performed using a HPGe detector GEMS8530P4 (85 mm crystal diameter, 50% relative efficiency, 1.90 keV FWHM resolution at 1332 keV), from ORTEC, connected to an ORTEC DSPEC jr 2.0 digital spectrometer for data acquisition. Silicon was placed with one of the four rectangular faces on a plastic container located at the center of the end-cap with its longitudinal axis perpendicular to the detector axis. Cu wire was instead fixed on a different counting plastic container in the same position with respect to the center of the end-cap, but it was lift up thanks to a plastic support in order to find the wire longitudinal axis at the same height of sample one with respect to the detector.

Peak areas were fitted with ROI32 algorithm of Gamma Vision software. Six channels were used for background calculation within the region of interest of the standard peak while for the ^{64}Cu peak

of the sample just two channels were used (one per side). This choice was forced to limit the interference of the 1342.2 keV ^{28}Mg peak ($t_{1/2}$ = 20.9 h) produced by ^{29}Si probably via the threshold reaction ^{29}Si(n,2p)^{28}Mg.

The contribution to the combined uncertainty due to counting statistics was in the range between 1% and 3%. The remaining contribution was due to geometry and positioning of the silicon sample and Cu wire; in fact, apart from the different shape of sample and standard, for which a 15% standard uncertainty was assigned, also a minimum misalignment of the wire in comparison to the center of mass of sample can yield a severe deviation in the detected number of counts, due to the extremely close counting position. In detail, a homogeneous ±2 mm variation was accounted for vertical position.

Six Cu measurements were carried out in consecutive steps of the protocol using two approaches in parallel: the relative and the k_0 method. The latter was performed in a particular way: in fact, silicon sample itself, from activation of 0.031 mol mol^{-1} abundant ^{30}Si isotope, was used as an internal comparator to quantify Cu amount. The great advantage brought with k_0-method was the complete absence of position and geometry effects during the γ-counting; this is particularly important when the sample is located very close to the detector. Moreover, both emission from ^{31}Si and ^{64}Cu were not affected by true coincidences and their energies, higher than 1 MeV, made self-absorption effects negligible.

4. Results

In this chapter, the results obtained in the experiments are showed. Every uncertainty budget here reported followed the guidelines suggested in the Guide to expression of Uncertainty on Measurement (GUM).[44]

4.1 The ^{30}Si mole fraction

The value of $x(^{30}\mathrm{Si})$ mole fraction was obtained by applying the relative INAA measurement model previously reported (eq. 21). As the final measurement model was multiplicative, the relative combined variance was calculated by summing the relative variances, obtained from relative uncertainties, for all the parameters.

Table 1: Uncertainty budget of $x(^{30}\mathrm{Si})$ evaluation of enriched sample.

quantity	unit	value	std uncertainty	index
X_i	$[X_i]$	x_i	$u(x_i)$	%

κ_{ti}	1	0.4243	0.0018	8.0
κ_{td}	1	0.0001502	0.0000013	33.5
κ_R	1	1.0281	0.0058	13.5
κ_ε	1	1.000	0.003	4.1
κ_{ss}	1	0.9944	0.0001	0.0
κ_{sa}	1	1.0000	0.0001	0.0
κ_g	1	1.0000	0.0001	0.0
$C_s(t_d)$	s^{-1}	5.617	0.053	37.6
$C_n(t_d)$	s^{-1}	19.900	0.046	2.3
$x(^{30}Si_n)$	mol mol^{-1}	0.031031	0.000048	1.0
m_n	g	13.5496	0.0001	0.0
m_s	g	13.5073	0.0001	0.0
M_s	g mol^{-1}	27.976933	0.000004	0.0
M_n	g mol^{-1}	28.08570	0.00021	0.0
Y	$[Y]$	Y	$u(y)$	%
$x(^{30}Si_s)$	mol mol^{-1}	0.0000005701	0.0000000088	100.0

The mole fraction value of isotope ^{30}Si, measured with relative method INAA, resulted to be 5.701(88) × 10^{-7} mol mol^{-1}. This value was close to but not in agreement with the 5.984(34) × 10^{-7} mol mol^{-1} value obtained by PTB, using IDMS, on a sample cut from the same region of the original crystal.[45](Figure 6)

Figure 6: Comparison between $x(^{30}Si)$ of enriched silicon material performed with INAA (reported in this study) and with IDMS by PTB, uncertainty bars account for k=2 coverage factor.

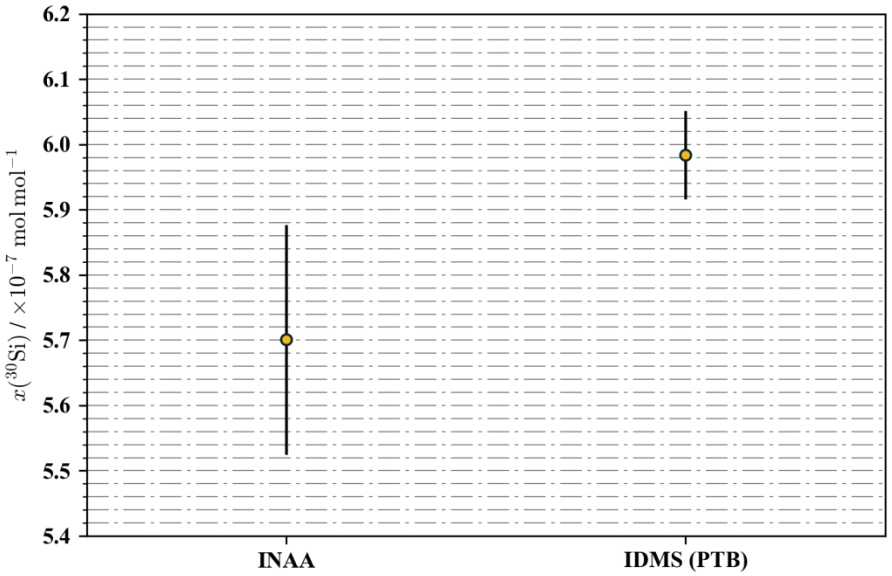

4.2 Bulk contamination

The investigation on bulk contamination included sixty-four possible contaminant elements. From the two irradiations scheduled (a short and a long one to cover the widest possible range of radionuclide's half-lives), nine elements (^{50}Cr, ^{59}Co, ^{63}Cu, ^{71}Ga, ^{75}As, ^{81}Br, ^{139}La, ^{186}W, and ^{197}Au) were quantified in a range from 6.9(12) × 10^{-10} g g^{-1} (Cu) to 3.02(38) × 10^{-14} g g^{-1} (Au) corresponding to a total mass deficit of -0.70(12) × 10^{-9} kg on a kilogram sphere under the hypothesis that all these contaminants are interstitial point defects and were homogeneously distributed along the float-zone Si batch. For the remaining elements, a detection limit was calculated ranging from 7.0 × 10^{-3} g g^{-1} (S) to 4.5 × 10^{-16} g g^{-1} (Ir). Results about all investigated elements are shown (Table 2); for convenience, concentration was expressed in mass fraction and also in number density (N_s) through the conversion $N_s = \frac{\rho_s \, d \, N_A}{M_s}$, where density of enriched silicon sample (d), molar mass of element (M_s) and N_A were retrieved from literature with negligible uncertainty.[46]

Table 2: Results for bulk contamination of silicon crystal: $t_{1/2}$ is the half-life of radionuclide, θ is the isotopic abundance of target atom, γ indicates the analytical gamma line detected, irradiation indicates whether the result derived from the short or the long neutron exposure (* indicates that result was calculated from spectra of the long irradiation acquired before deep etching), ρ_s and N_s are the concentration of element in mass fraction and number density, respectively.

reaction	$t_{1/2}$[31]	θ(is)[31]	γ[31] / keV	irradiation	ρ_s / g g^{-1}	N_s / cm^{-3}
^{23}Na(n,γ)^{24}Na	14.96 h	1.000	2754	short	≤9.7 × 10^{-12}	≤5.9 × 10^{11}
^{26}Mg(n,γ)^{27}Mg	9.462 min	0.11	843.8	short	≤3.0 × 10^{-7}	≤1.7 × 10^{16}
^{36}S(n,γ)^{37}S	5.05 min	0.0002	3103.4	short	≤7.0 × 10^{-3}	≤3.1 × 10^{20}
^{37}Cl(n,γ)^{38}Cl	37.24 min	0.2423	2167.4	short	≤2.2 × 10^{-10}	≤8.8 × 10^{12}
^{40}Ar(n,γ)^{41}Ar	1.822 h	0.996	1293.6	short	≤8.9 × 10^{-12}	≤3.1 × 10^{11}
^{41}K(n,γ)^{42}K	12.36 h	0.0673	1524.7	short	≤1.6 × 10^{-11}	≤5.6 × 10^{11}
^{46}Ca(n,γ)^{47}Sc	3.349 d	0.000035	159.4	long	≤6.3 × 10^{-10}	≤2.2 × 10^{13}
^{45}Sc(n,γ)^{46}Sc	83.83 d	1.0000	889.3	long	≤2.5 × 10^{-15}	≤7.9 × 10^{7}
^{50}Ti(n,γ)^{51}Ti	5.76 min	0.052	320.1	short	≤4.5 × 10^{-8}	≤1.3 × 10^{15}
^{51}V(n,γ)^{52}V	3.75 min	0.9975	1434.1	short	≤1.8 × 10^{-9}	≤5.0 × 10^{13}
^{50}Cr(n,γ)^{51}Cr	27.7 d	0.0435	320.1	long	1.40(14) × 10^{-12}	3.76(38) × 10^{10}
^{55}Mn(n,γ)^{56}Mn	2.579 h	1.0000	846.8	short	≤7.1 × 10^{-13}	≤1.8 × 10^{10}
^{58}Fe(n,γ)^{59}Fe	44.5 d	0.0028	1099.3	long	≤2.6 × 10^{-11}	≤6.4 × 10^{11}
^{59}Co(n,γ)^{60}Co	1925.3 d	1.0000	1332.5	long	7.6(15) × 10^{-14}	1.81(34) × 10^{9}
^{64}Ni(n,γ)^{65}Ni	2.517 h	0.0091	1115.5	short	≤2.8 × 10^{-9}	≤6.6 × 10^{13}
^{63}Cu(n,γ)^{64}Cu	12.7 h	0.6917	1345.8	long*	6.9(12) × 10^{-10}	1.52(27) × 10^{13}
^{64}Zn(n,γ)^{65}Zn	244.3 d	0.486	1115.5	long	≤1.4 × 10^{-12}	≤3.0 × 10^{10}
^{71}Ga(n,γ)^{72}Ga	14.1 h	0.399	834	long*	3.1(10) × 10^{-13}	6.2(20) × 10^{9}
^{76}Ge(n,γ)^{77}Ge	11.3 h	0.078	264.4	long*	≤3.2 × 10^{-10}	≤6.2 × 10^{12}

$^{75}As(n,\gamma)^{76}As$	26.24 h	1.0000	559.2	short	$1.28(47) \times 10^{-12}$	$2.39(87) \times 10^{10}$
$^{74}Se(n,\gamma)^{75}Se$	119.781 d	0.0089	136	long	$\leq 2.6 \times 10^{-13}$	$\leq 4.6 \times 10^{9}$
$^{81}Br(n,\gamma)^{82}Br$	35.3 h	0.4931	554.3	long*	$1.80(30) \times 10^{-13}$	$3.15(52) \times 10^{9}$
$^{85}Rb(n,\gamma)^{86}Rb$	18.63 d	0.7217	1077	long	$\leq 1.7 \times 10^{-12}$	$\leq 2.8 \times 10^{10}$
$^{84}Sr(n,\gamma)^{85}Sr$	64.84 d	0.0056	514	long	$\leq 1.8 \times 10^{-11}$	$\leq 2.9 \times 10^{11}$
$^{89}Y(n,\gamma)^{90m}Y$	3.19 h	1.0000	479.5	short	$\leq 1.5 \times 10^{-8}$	$\leq 2.3 \times 10^{14}$
$^{94}Zr(n,\gamma)^{95}Zr$	62.02 d	0.1728	756.7	long	$\leq 1.9 \times 10^{-11}$	$\leq 2.9 \times 10^{11}$
$^{93}Nb(n,\gamma)^{94m}Nb$	6.26 min	1.0000	871	short	$\leq 2.3 \times 10^{-5}$	$\leq 3.5 \times 10^{17}$
$^{98}Mo(n,\gamma)^{99m}Tc$	6.01 h	0.2413	140.5	long	$\leq 5.2 \times 10^{-12}$	$\leq 7.6 \times 10^{10}$
$^{102}Ru(n,\gamma)^{103}Ru$	39.35 d	0.316	497.1	long	$\leq 1.8 \times 10^{-13}$	$\leq 2.4 \times 10^{9}$
$^{108}Pd(n,\gamma)^{109}Pd$	13.36 h	0.2646	309.1	long*	$\leq 8.0 \times 10^{-12}$	$\leq 1.1 \times 10^{11}$
$^{109}Ag(n,\gamma)^{110m}Ag$	249.8 d	0.4817	657.8	long	$\leq 2.2 \times 10^{-13}$	$\leq 2.8 \times 10^{9}$
$^{114}Cd(n,\gamma)^{115}Cd$	53.46 h	0.2872	527.9	long*	$\leq 1.2 \times 10^{-12}$	$\leq 1.5 \times 10^{10}$
$^{115}In(n,\gamma)^{116}In$	54.41 min	0.957	1293.5	short	$\leq 1.8 \times 10^{-13}$	$\leq 2.2 \times 10^{9}$
$^{116}Sn(n,\gamma)^{117m}Sn$	13.6 d	0.147	158.5	long	$\leq 3.5 \times 10^{-11}$	$\leq 4.2 \times 10^{11}$
$^{123}Sb(n,\gamma)^{124}Sb$	60.2 d	0.427	602.7	long	$\leq 6.3 \times 10^{-14}$	$\leq 7.2 \times 10^{8}$
$^{130}Te(n,\gamma)^{131}I$	8.021 d	0.338	364.5	long	$\leq 9.9 \times 10^{-13}$	$\leq 1.1 \times 10^{10}$
$^{127}I(n,\gamma)^{128}I$	24.99 min	1.0000	442.9	short	$\leq 9.5 \times 10^{-11}$	$\leq 1.1 \times 10^{12}$
$^{133}Cs(n,\gamma)^{134}Cs$	754.2 d	1.0000	604.7	long	$\leq 4.1 \times 10^{-14}$	$\leq 4.4 \times 10^{8}$
$^{130}Ba(n,\gamma)^{131}Ba$	11.5 d	0.00106	496.3	long*	$\leq 1.5 \times 10^{-11}$	$\leq 1.5 \times 10^{11}$
$^{139}La(n,\gamma)^{140}La$	1.678 d	0.9991	1596.2	long*	$7.14(71) \times 10^{-14}$	$7.18(71) \times 10^{8}$
$^{140}Ce(n,\gamma)^{141}Ce$	32.51 d	0.8848	145.4	long	$\leq 1.7 \times 10^{-13}$	$\leq 1.7 \times 10^{9}$
$^{141}Pr(n,\gamma)^{142}Pr$	19.12 h	1.0000	1575.6	long*	$\leq 7.3 \times 10^{-13}$	$\leq 7.2 \times 10^{9}$
$^{146}Nd(n,\gamma)^{147}Nd$	10.98 d	0.1719	91.1	long	$\leq 6.5 \times 10^{-13}$	$\leq 6.3 \times 10^{9}$
$^{152}Sm(n,\gamma)^{153}Sm$	46.5 h	0.266	103.2	long*	$\leq 5.7 \times 10^{-15}$	$\leq 5.3 \times 10^{7}$
$^{151}Eu(n,\gamma)^{152}Eu$	4945.4 d	0.4786	121.8	long	$\leq 5.1 \times 10^{-15}$	$\leq 4.7 \times 10^{7}$
$^{152}Gd(n,\gamma)^{153}Gd$	240.4 d	0.002	97.4	long	$\leq 5.8 \times 10^{-13}$	$\leq 5.2 \times 10^{9}$
$^{159}Tb(n,\gamma)^{160}Tb$	72.3 d	1.0000	298.6	long	$\leq 1.8 \times 10^{-14}$	$\leq 1.6 \times 10^{8}$
$^{164}Dy(n,\gamma)^{165}Dy$	2.334 h	0.281	94.7	short	$\leq 1.3 \times 10^{-12}$	$\leq 1.2 \times 10^{10}$
$^{165}Ho(n,\gamma)^{166}Ho$	26.83 h	1.0000	80.6	long*	$\leq 6.1 \times 10^{-14}$	$\leq 5.2 \times 10^{8}$
$^{170}Er(n,\gamma)^{171}Er$	7.516 h	0.149	308.3	long*	$\leq 1.1 \times 10^{-11}$	$\leq 9.3 \times 10^{10}$
$^{169}Tm(n,\gamma)^{170}Tm$	128.6 d	1.0000	84.3	long	$\leq 5.8 \times 10^{-15}$	$\leq 4.8 \times 10^{7}$
$^{174}Yb(n,\gamma)^{175}Yb$	4.185 d	0.3183	396.3	long*	$\leq 2.6 \times 10^{-14}$	$\leq 2.1 \times 10^{8}$
$^{176}Lu(n,\gamma)^{177}Lu$	6.73 d	0.0259	208.4	long	$\leq 1.3 \times 10^{-14}$	$\leq 1.1 \times 10^{8}$
$^{180}Hf(n,\gamma)^{181}Hf$	42.39 d	0.3522	482.2	long	$\leq 2.9 \times 10^{-14}$	$\leq 2.3 \times 10^{8}$
$^{181}Ta(n,\gamma)^{182}Ta$	114.4 d	0.9999	67.8	long	$\leq 3.6 \times 10^{-14}$	$\leq 2.8 \times 10^{8}$
$^{186}W(n,\gamma)^{187}W$	23.72 h	0.2864	685.7	long*	$6.87(42) \times 10^{-12}$	$5.22(32) \times 10^{10}$
$^{185}Re(n,\gamma)^{186}Re$	3.718 d	0.374	137.2	long*	$\leq 2.7 \times 10^{-14}$	$\leq 2.0 \times 10^{8}$
$^{190}Os(n,\gamma)^{191}Os$	15.4 d	0.264	129.4	long	$\leq 5.2 \times 10^{-14}$	$\leq 3.8 \times 10^{8}$
$^{191}Ir(n,\gamma)^{192}Ir$	73.827 d	0.373	316.5	long	$\leq 4.5 \times 10^{-16}$	$\leq 3.3 \times 10^{6}$
$^{198}Pt(n,\gamma)^{199}Au$	3.139 d	0.072	158.4	long*	$\leq 1.2 \times 10^{-12}$	$\leq 8.5 \times 10^{9}$
$^{197}Au(n,\gamma)^{198}Au$	2.695 d	1.0000	411.8	long	$3.02(38) \times 10^{-14}$	$2.14(27) \times 10^{8}$

$^{202}Hg(n,\gamma)^{203}Hg$	46.61 d	0.297	279.2	long	$\leq 9.4 \times 10^{-14}$	$\leq 6.5 \times 10^{8}$
$^{232}Th(n,\gamma)^{233}Pa$	26.97 d	1.0000	311.9	long	$\leq 3.1 \times 10^{-14}$	$\leq 1.8 \times 10^{8}$
$^{238}U(n,\gamma)^{239}Np$	2.357 d	0.9928	106.1	long*	$\leq 1.6 \times 10^{-13}$	$\leq 9.5 \times 10^{8}$

The results are also summarized in Figure 7 which clearly distinguishes between quantified elements and detection limits ranges of non-quantified analytes.

Figure 7: Summary of contamination analysis performed on ^{28}Si-enriched silicon material; the total number of investigated elements was sixty-four.

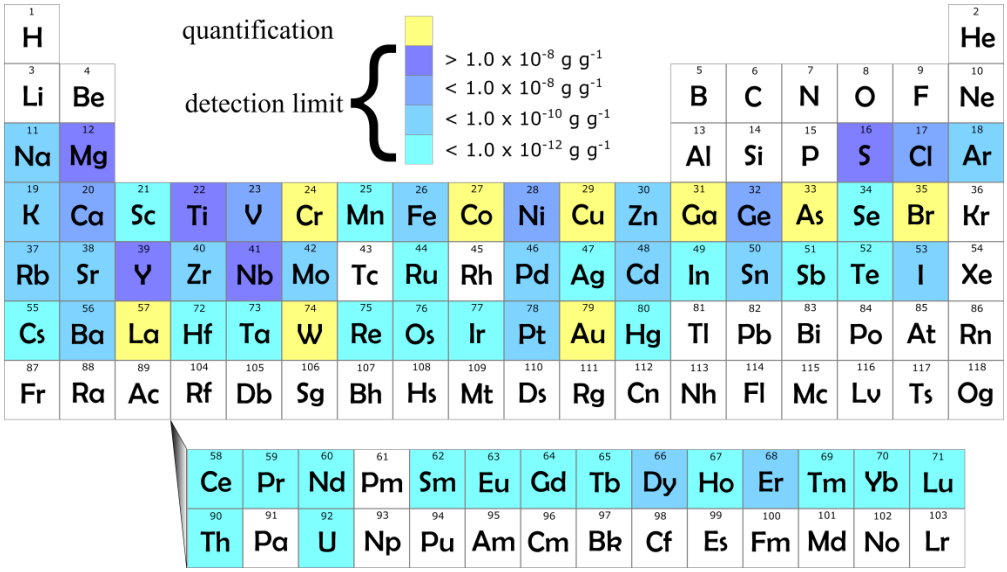

4.3 Vacancies concentration

The Cu trends resulted to be in agreement with both adopted analytical methods. (Figure 8) However assessments carried out with k_0-method showed much lower uncertainty. This outcome is unusual as, in general, relative INAA shows lower uncertainties than k_0-INAA; in this particular case, the matrix and shape of Cu wire standard were so different comparatively with the silicon sample, that relative INAA dealt with very important corrections that heavily affected the combined uncertainty.

Figure 8: Cu trend within cycles of copper decoration procedure analyzed with NAA exploiting both relative and k_0 method, uncertainty bars account for k=2 coverage factor.

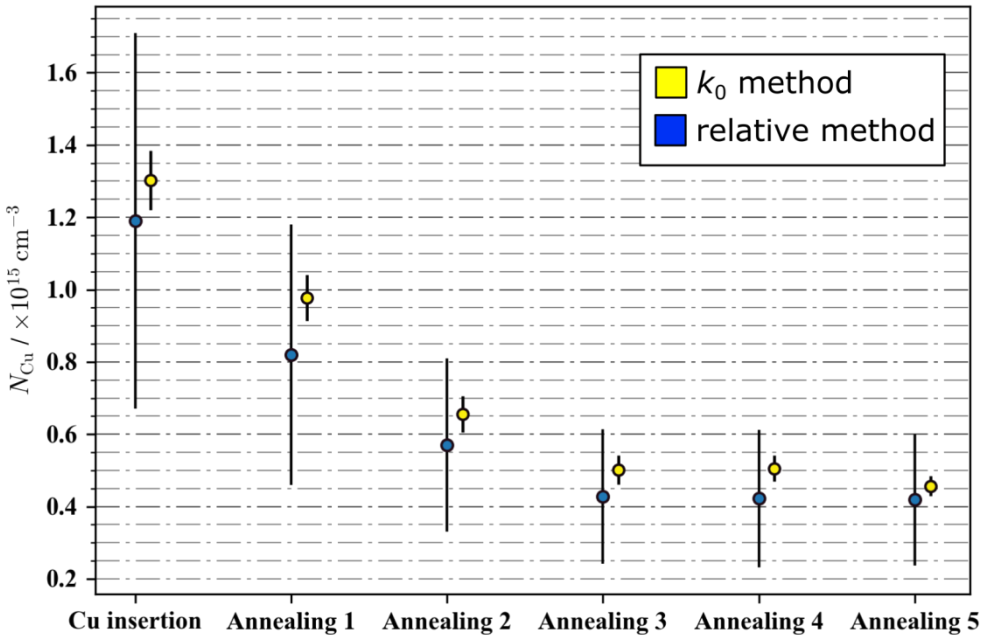

The last three points in Figure 8 showed a plateau meaning that no further out-diffusion of copper occurred; Cu amount was, thus, exclusively due to the precipitated Cu_3Si within the silicon crystal. From eq. 27, estimate of upper limit for vacancies concentration was yielded: at the plateau a value less than 1×10^{14} cm^{-3} was obtained.

Uncertainty budget was evaluated through propagation of relative variances of all input parameters (eq. 26); an example of budget is reported afterwards. (Table 3)

Table 3: Uncertainty budget for a single N_{Cu} quantification obtained during the 4th annealing cycle with the relative standardization.

quantity X_i	unit $[X_i]$	value x_i	std uncertainty $u(x_i)$	index %
κ_{td}	1	0.001344	0.000001	0.0
κ_R	1	1.000	0.0030	1.8
κ_ε	1	1.000	0.096	18.0
κ_{ss}	1	1.0030	0.0006	0.0
κ_{sa}	1	0.9920	0.0016	0.0
κ_g	1	1.0	0.2	78.4
$C_s(t_d)$	s^{-1}	0.1393	0.0042	1.8
$C_n(t_d)$	s^{-1}	3.328	0.009	0.0
m_n	g	0.00326	0.00001	0.0
m_s	g	9.53807	0.00001	0.0
d_s	g cm^{-3}	2.329	0.001	0.0
M_n	g mol^{-1}	63.546	0.003	0.0

N_A	mol^{-1}	6.022×10^{23}	0.000	0.0
Y	$[Y]$	Y	$u(y)$	%
N_{Cu}	$g\ cm^{-3}$	4.22×10^{14}	0.95×10^{14}	100.0

5. Discussion

INAA proved to be a powerful tool in order to perform the analysis of the silicon materials used in the framework of the redefinition of Avogadro constant and the *mise en pratique* of the new kg and mol definitions with silicon route (production of silicon crystals characterized with XRCD). Measurement methods were developed and applied to study the molar mass (through quantification of ^{30}Si minor abundant isotope), the elemental contamination and the presence of vacancies.

The $x(^{30}Si)$ value obtained in this study corroborated the analysis performed by PTB with IDMS on a sample of the same single crystal and the corresponding M value, one of the input parameters of XRCD experiment.

For what concerns the purity of silicon material, the obtained results pointed out that the new material[47] has a lesser amount of elemental contamination in comparison to the previous enriched silicon crystal[41] used for the latest determination of the Avogadro constant. In addition, also for undetected elements, the analysis achieved detection limits generally of 1 order of magnitude lower with exception of some short half-life radionuclides. The optimization of method played a fundamental role to the decrease of detection limits for long half-lives. On the other hand, the need to perform a post-irradiation etching prevented the possibility to improve detection also for short-lived radionuclides.

Probably, the greater care during manufacturing or even the particularly high ^{28}Si-enrichment reached during the production might have contributed to the purification. Anyway, for the most part of periodic table (including also, B, N, C, O, P, non-revealed with INAA), it has been demonstrated that amount of contaminants represents a negligible part of the correction on mass quantification of the new silicon material.

Performing the purity and $x(^{30}Si)$ measurement analyses in the Australian OPAL reactor was advantageous due to the extremely high and thermalized neutron flux which translated in major activity of radioisotopes of interest and lesser side reactions; in fact, with the lower intensity of neutron flux and poor thermalization available at the Pavia's TRIGA, the detection limits would have been higher. Preliminary test analysis previously developed at TRIGA facility on older and less enriched material showed that optimization of method approached its limit due to the technical limitations of the reactor itself.

Upper limit for vacancies concentration was evaluated by application of INAA to the copper decoration method. Feasibility test performed on a single crystal of natural isotopic abundance proved that INAA can be capable to detect Cu concentration at appreciable level to quantify voids within the crystal with tolerable uncertainty. As the investigated natural crystal was produced with the same technique (float zone) than enriched ones, vacancies concentration is expected to be similar. Reduction of uncertainty on results obtained from relative method will be convenient but not compulsory due to the very low contribution to the N_A uncertainty. To this scope, an improving strategy can involve the dissolution of Cu standard with HNO_3 in a vial with similar dimensions of the silicon sample; in this case the almost totality of geometry and positioning issues are solved. Use of k_0 method instead would be challenging due to the ultra-trace amount of the ^{30}Si comparator. A further issue derived from lattice damage induced by neutrons during irradiation[48], might be solved by limiting neutron fluence towards the sample by decreasing exposure time or neutron flux intensity.

To sum up, data collected from the characterization of newly produced silicon material will be part of information required for the ongoing N_A redetermination through the XRCD route.[49] Finally, redefinition of kg and mol, foreseen before the end of 2018, will be officially complete when perfect agreement (within the target 2×10^{-8} relative uncertainty) between h and N_A will be achieved from the two different approaches (XRCD and Kibble balance). To this aim analytical methods based on NAA proved to be a valuable source of information concerning characterization of this particular material involved in redetermination of N_A.

7. Acknowledgment

Figure 5 and Table 1 are reprinted or adapted with permission from Di Luzio *et al*; "Measurement of the ^{30}Si mole fraction in the new Avogadro silicon material by Neutron Activation and high resolution γ-spectrometry", *Analytical Chemistry*, **2017**; 89, 6726-6730. Copyright 2017 American Chemical Society.

Figure 7 and Table 2 are reprinted or adapted with permission from Di Luzio *et al*; "Impurities in a ^{28}Si-enriched single crystal produced for the realization of the redefined kilogram", *Analytical Chemistry*, **2017**; 89, 6314-6317. Copyright 2017 American Chemical Society.

Figure 8 and Table 3 are reprinted or adapted with permission from D'Agostino *et al*; "Quantification of the void volume in single-crystal silicon", *Analytical Chemistry*, **2016**; 88, 11678-11683. Copyright 2016 American Chemical Society.

The author wishes to acknowledge Giovanni Mana for the valuable support and discussion in the framework of characterization of silicon material.

The author wishes to acknowledge John Bennett and Attila Stopic for the intense collaboration culminated in the experiments performed at ANSTO. Moreover, a special thanks is addressed to the neutron reactor operators of ANSTO.

The author wishes to acknowledge Michele Prata, Daniele Alloni and Giovanni Magrotti and all the staff of Laboratorio di Energia Nucleare Applicata (LENA) for the good outcome of irradiations performed in the TRIGA Mark II reactor and valuable technical assistance.

This work was funded by the Italian Ministry of Education, University, and Research (awarded project P6-2013, implementation of the new SI).

8. Bibliography

[1] International Vocabulary of Metrology (VIM), BIPM: Sèvres, France, **2008**.

[2] http://www.bipm.org/en/worldwide-metrology/metre-convention/official-texts/

[3] The International System of Units (SI), 8th ed.; BIPM: Sèvres, France, **2006** (updated in 2014).

[4] Quinn T J; "News from the BIPM", *Metrologia*, **1996**; 33, 81-89 (Resolution 5).

[5] Girard G; "The third periodic verification of National Prototypes of the kilogram", *Metrologia*, **1994**; 31, 317-336.

[6] http://www.bipm.org/en/si-download-area/graphics-files.html

[7] Wheatley N; "On the dimensionality of the Avogadro constant and the definition of the mole", *Metrologia*, **2011**; 48, 71-82.

[8] Leonard B P; "On the role of the Avogadro constant in redefining SI units for mass and amount of substance", *Metrologia*, **2007**; 44, 82-86.

[9] SI Brochure published following adoption of the "New SI", 9th ed.; BIPM: Sèvres, France, **2016** (draft).

[10] Robinson I A; "Towards the redefinition of the kilogram: a measurement of the Planck constant using the NPL Mark II watt balance", *Metrologia*, **2012**; 49, 113-156.

[11] Davies R S; "What is a kilogram in the revised International System of units (SI)?", *Journal of Chemical Education*, **2015**; 92, 1604-1609.

[12] Andreas B, Azuma Y, Bartl G, Becker P, Bettin H, Borys M, Busch I, Fuchs P, Fujii K, Fujimoto H, Kessler E, Krumrey M, Kuetgens U, Kuramoto N, Mana G, Massa E, Mizushima S, Nicolaus A, Picard A, Pramann A, Rienitz O, Schiel D, Valkiers S, Waseda A, Zakel S; "Counting the atoms in a ^{28}Si single crystal from a new kilogram definition", *Metrologia*, **2011**; 48, S1-S13.

[13] Massa E, Mana G, Kuetgens U, Ferroglio L; "Measurement of the {220} lattice-plane of a ^{28}Si x-ray interferometer", *Metrologia*, **2011**; 48, S37-S43.

[14] Picard A, Barat P, Borys M, Firlus M, Mizushima S; "State-of-the-art mass determination of ^{28}Si spheres for the Avogadro project", *Metrologia*, **2011**; 48, S112-S119.

[15] Rienitz O, Pramann A, Schiel D; "Novel concept for the mass spectrometric determination of absolute isotopic abundances with improved measurement uncertainty: Part 1 – theoretical derivation and feasibility study", *International Journal of Mass Spectrometry*, **2010**; 289, 47-53.

[16] Cameron I R; Nuclear fission reactors, Plenum Press, New York, **1982**.

[17] Greenberg R, Bode P, De Nadai Fernandes E A; "Neutron Activation Analysis: a primary method of measurement", *Spectrochimica Acta part B*, **2011**; 66, 193-241.

[18] De Corte F, Moens L, Sordo-El Hammami K, Simonits A, Hoste J; "Modification and generalization of some methods to improve the accuracy of α-determination in the $1/E^{1+\alpha}$ epithermal neutron spectrum", *Journal of Radioanalytical and Nuclear Chemistry*, **1979**; 52, 305-316.

[19] Ryves T B; "A new thermal neutron flux convention", *Metrologia*, **1969**; 5, 119-124.

[20] De Corte F; The k_0-standardization method. A move to the optimization of neutron activation analysis, Rijksuniversiteit, Gent, **1987**.

[21] De Corte F, Bellemans F, De Neve P, Simonits A; "The use of a modified Westcott-formalism in the k_0-standardization of the NAA: the state of affairs", *Journal of Radioanalytical and Nuclear Chemistry*, **1994**; 179, 93-103.

[22] van Sluijs R, Jacimovic R, Kennedy G; "A simplified method to replace Westcott formalism in k_0-NAA using non-1/*v* nuclides", *Journal of Radioanalytical and Nuclear Chemistry*, **2014**; 300, 539-545.

[23] Chillian C, Lacroix C; "Towards routine NAA of materials rich in heavy elements with iterative gamma-ray attenuation and neutron self-shielding calculations", *Journal of Radioanalytical and Nuclear Chemistry*, **2014**; 300, 547-552.

[24] Mejia J, Coplen T B, Berglund M, Brand W A, De Bièvre P, Gröning M, Holden N E, Irrgeher J, Loss R D, Walczyk T, Prohaska T; "Atomic weights of the elements 2013 (IUPAC Technical Report)", *Pure and Applied Chemistry*, **2016**; 88, 265-291.

[25] Vocke R D *Jr*, Rabb S A, Turk G C; "Absolute silicon molar mass measurement, the Avogadro constant and the redefinition of the kilogram", *Metrologia*, **2014**; 51, 361-375.

[26] Tuli J K; Nuclear Wallet Cards, Brookheaven National Laboratory: Upton (New York), USA, **2008**.

[27] Ouellet C, Singh B; "Nuclear Data Sheets for A=31", *Nuckear Data Sheets*, **2013**; 114, 209-396.

[28] D'Agostino G, Di Luzio M, Mana G, Oddone M, Pramann A, Prata M; "The ^{30}Si mole fraction of a silicon material highly enriched in ^{28}Si determined by Instrumental Neutron Activation Analysis", *Analytical Chemistry*, **2015**; 87, 5716-5722.

[29] D'Agostino G, Di Luzio M, Mana G, Oddone M; "A new low-uncertainty measurement of the ^{31}Si half-life", *Metrologia*, **2017**; 54, 410-416.

[30] Zakel S, Wundrack S, Niemann H, Rienitz O, Schiel D; "Infrared spectrometric measurement of impurities in highly enriched 'Si28'", *Metrologia*, **2011**; 48, S14-S19.

[31] D'Agostino G, Bergamaschi L, Giordani L, Mana G, Massa E, Oddone M; "Elemental characterization of the Avogadro silicon crystal WASO04 by Neutron Activation Analysis", *Metrologia*, **2012**; 49, 696-701.

[32] Girardi F, Guzzi G, Pauly J; "Reactor Neutron Activation Analysis by the single comparator method", *Analytical Chemistry*, **1965**; 37, 1085-1092.

[33] k_0-Nuclear Data Subcommittee of k_0-International Scientific Committee. Database of Recommended k_0-Data; released January 11, 2016.

[34] Pethrick R A; "Positron annihilation – A probe for nanoscale voids and free volume?", *Progress in Polymer Science*, **1997**; 22, 1-47.

[35] Spaepen F, Eliat A; "New methods for determining the void content of silicon single crystal", *IEEE Transactions on Instrumentation and Measurement*, **1999**; 48, 230-232.

[36] Abrosimov N V, Aref'ev D G, Becker P, Bettin H, Bulanov A D, Churbanov M F, Filimonov S V, Gavva V A, Godisov O N, Gusev A V, Kotereva T V, Nietzold D, Peters M, Potapov A M, Pohl H-J, Pramann A, Riemann H, Scheel P-T, Stosch R, Wundrack S, Zakel S; "A new generation of 99.999% enriched ^{28}Si single crystals for the determination of Avogadro's constant", *Metrologia*, **2017**; in press.

[37] D'Agostino G, Mana G, Oddone M, Prata M, Bergamaschi L, Giordani L; "Neutron Activation Analysis of the ^{30}Si content of highly enriched ^{28}Si: proof of concept and estimation of the achievable uncertainty", *Metrologia*, **2014**; 51, 354-360.

[38] Martinho E, Salgado J, Gonçalves I F; "Universal curve of the thermal neutron self-shielding factor in foils, wires, spheres and cylinders" *Journal of Radioanalytical and Nuclear Chemistry*, **2004**; 261, 637-643.

[39] Martinho E, Gonçalves I F, Salgado J; "Universal curve of epithermal neutron resonance self-shielding factors in foils, wires and spheres" *Applied Radiation and Isotopes*, **2003**; 58, 371-375.

[40] D'Agostino G, Di Luzio M, Mana G, Oddone M, Bennett J W, Stopic A; "Purity of 28Si-enriched silicon material used for the determination of the Avogadro constant", *Analytical Chemistry*, **2016**; 88, 6881-6888.

[41] Currie L A; "Limits for qualitative detection and quantitative determination. Application to radiochemistry", *Analytical Chemistry*, **1968**; 40, 586-593.

[42] van Sluijs R, Stopic A, Jacimovic R; "Evaluation of Westcott $g(T_n)$-factors used in k_0-NAA for "non-1/*v*" (n,γ) reactions", *Journal of Radioanalytical and Nuclear Chemistry*, **2015**; 306, 579-587.

[43] Di Luzio M, Oddone M, Prata M, Alloni D, D'Agostino G; "Measurement of the neutron flux parameters *f* and α at the Pavia TRIGA Mark II reactor", *Journal of Radioanalytical and Nuclear Chemistry*, **2017**; 312, 75-80.

[44] Guide to the expression of Uncertainty in Measurement (GUM), BIPM: Sèvres, France, **2008**.

[45] Pramann A, Narukawa T, Rienitz O; "Determination of the isotopic composition and molar mass of a new 'Avogadro'-crystal: aspects in terms of homogeneity and enrichment-related uncertainty reduction", *Metrologia*, Submitted.

[46] Azuma Y, Barat P, Bartl G, Bettin H, Borys M, Busch I, Cibik L, D'Agostino G, Fujii K, Fujimoto H, Hioki A, Krumrey M, Kuetgens U, Kuramoto N, Mana G, Massa E, Meeß R, Mizushima S, Narukawa T, Nicolaus A, Pramann A, Rabb S A, Rienitz O, Sasso C P, Stock M, Vocke R D *Jr*, Waseda A, Wundrack S, Zakel S; "Improved measurement results for the Avogadro constant using a ^{28}Si-enriched crystal" *Metrologia*, **2015**; 52, 360-375.

[47] Pramann A, Rienitz O; "Mass spectrometric investigation of silicon extremely enriched in ^{28}Si: from $^{28}SiF_4$ (gas phase IRMS) to ^{28}Si crystals (MC-ICP-MS)", *Analytical Chemistry*, **2016**; 88, 5963-5970.

[48] Newman R C; "Defects in silicon", *Reports on Progress in Physics*, **1982**; 45, 1163-1210.

[49] Bartl G, Becker P, Beckhoff B, Bettin H, Beyer E, Borys M, Busch I, Cibik L, D'Agostino G, Darlatt E, Di Luzio M, Fukii K, Fujimoto H, Fujita K, Kolbe M, Krumrey M, Kuramoto N, Massa E, Mecke M, Mizushima S, Müller M, Narukawa T, Nicolaus A, Pramann A, Rauch D, Rienitz O, Sasso C P, Stopic A, Stosch R, Waseda A, Wundrack S, Zhang L, Zhang X W; "A new ^{28}Si single crystal: counting the atoms for the new kilogram definition", *Metrologia*, **2017**; 54, 693-715.